5

Weibull Model for Bimodular Cylindrical Specimen

5.1 Introduction

Designing structural components fabricated from ceramic materials are desirable in many applications because of their strength at elevated temperature, high thermal conductivity, low thermal expansion, and outstanding wear resistance. On the other hand, structural ceramics are generally brittle and are associated with low strain tolerance, low fracture toughness and thereby putting into effect a severe limitation on the size of the critical flaw or defect. As well, fracture strengths of identical specimens of ceramic materials vary considerably and therefore, failure predictions for ceramics are performed using statistics and reliability analysis. The most widely accepted statistical method for characterizing the strength behavior of brittle materials is Weibull analysis, which is based on the weakest link theory. Furthermore, as the volume and/ or surface area of a ceramic component under stress increases, the probability of encountering a critical flaw increases. This effect introduces a size dependence of strength. In other words, the strength of a brittle ceramic component depends on the stress distribution and the volume and/or surface area stressed in tension. Thus calculation of effective volume and effective surface is a key step in estimating reliability of ceramic

component life cycle. Most of the tests performed to evaluate the mechanical reliability of ceramic materials are conducted on small laboratory specimens. This is because the testing of actual large size components subjected to complex stress fields at high temperature is both expensive and tedious. Most common tests performed to assess the strength and reliability of ceramic components are bend bar specimens tested in three-point and four-point flexure, C-ring and O-ring specimen under diametral compressive or tensile loads and biaxial ring-on-ring specimens. Weibull effective volumes and surfaces are used to scale ceramic strength from one component size to another or from one loading configuration to another (Jadaan et al. 1991; Quinn and Morrell 1991; Shelleman et al. 1991; Duffy et al. 1992, 2005, Quinn 2003a, b).

Although the classical theory of elasticity assumes that materials have the same elastic properties in tension as well as in compression, numerous studies have indicated that materials like ceramic exhibit in a different way in tension and compression. With the developments of new materials, the numerical analyses incorporating the bi-modular properties are gaining attention of the researchers. The chance of failure is significantly affected by neutral axis shift due to the bi-modular property of the material. The effective volume and effective surface of bi-modular material subjected to flexural loading is significantly affected by the neutral axis shift. The phenomena of different behavior in tension and compression were initially recognized by Saint-Venant in 1864 (Saint-Venant 1864), however, the perception did not receive much attention for a long time. Later on, in 1941, the concept of a bi-modular material was revisited by Timoshenko while considering the flexural stress in such a material undergoing

pure bending(Timoshenko 1941). The bi-modular concept was extended to two-dimensional materials by Ambartsumyan (1965-69) (Ambartsumyan 1965, 1966, 1969). Since last few decades, several attempts have been made to establish constitutive relationships and exploring different aspects for such materials (Marin 1962; Isabekian and Khachatryan 1969; Tabaddor 1972; Kamiya 1975). Also, numerous literatures related to analytical and numerical solutions are available for the effective volume and effective surface area in beams with single modulus (Jadaan et al. 1991; Shelleman et al. 1991; Nemeth et al. 2005, 2013). However, computation of the effective volumes, surfaces and strength scaling of bi-modular material and thereby the more accurate reliability prediction remain really a challenging issue.

Although previous investigators have attempted to predict the mechanical behavior of one simple specimen configuration from another using Weibull statistics and tabulations of formulas for effective volume or effective surface for square or rectangular beam specimens as well as cylindrical rods loaded in flexure are readily available; however, to the best of the authors' knowledge closed form expressions of Weibull effective volumes and surfaces for bi-modular material are not reported in the literatures so far(Quinn 2003a, b; Duffy et al. 2005; Wereszczak et al. 2008). In the present work, effort has been made to derive closed form expressions of Weibull effective volume and effective surface for the cylindrical beam specimen having bi-modularity. Though, it has not been possible to obtain the completely closed form expression due to the occurrence of complex integral form, still, one can get rid of the extensive computer modeling efforts because of the development of semi analytical expressions of effective volume and effective surface. Effective volume and effective area were computed semi

analytically as a function of the Weibull modulus. As for the practical purposes, it is required to convert data rapidly between various loading configurations, therefore, expressions of strength scaling ratios and table of conversion factors, for strength scaling from one flexural loading configuration to another with varying Weibull modulus are also provided. For illustrative purposes, derivation of effective volumes and effective surfaces for three simple loading configurations are illustrated in this chapter.

5.2 Weibull Statistical Failure Analysis

Weibull statistical failure analysis is based on the weakest link theory and has been extensively used to describe the features of the strength of ceramic materials. According to this theory, the probability of failure (P_f) can be related to the strength of a specimen through the two-parameter Weibull equation

$$P_f = 1 - \exp\left[-\int_V \left(\frac{\sigma}{(\sigma_0)_V} \right)^m dV \right] \tag{5.1}$$

Eq 5.1 can be transformed into:

$$P_f = 1 - \exp\left[-\left(\frac{\sigma_{\max}}{(\sigma_0)_V} \right)^m \int_V \left(\frac{\sigma}{\sigma_{\max}} \right)^m dV \right]$$

Where,

$\sigma_{\max}$ =Maximum Stress

$\int_V \left(\frac{\sigma}{\sigma_{\max}} \right)^m dV = V_E$ =Effective Volume

Where, m is the Weibull modulus and associated with strength controlling flaws distributed through the volume; $(\sigma_0)_V$ is the Weibull material scale parameter and can be described as the Weibull characteristic strength of a hypothetical test specimen with unit volume loaded in uniform uniaxial tension; σ is the failure stress.

Now, this probability of failure can be estimated from the following expression:

$$P_f = \frac{n-0.5}{N} \tag{5.2}$$

where P_f is the cumulative probability according to ranking of a set of failure strength data, n is the rank of the individual specimen arranged in increasing order of failure strength and *N* is the total number of specimens tested. The probability of failure against tensile strength data set has been plotted with 90% confidence bound for all the three estimator**.** The scattered data on the Weibull plot has been analyzed using the best fit line drawn by least square estimator (LIN2), biased (MLE2-B) and unbiased (MLE2-U) maximum likelihood estimator procedure.

Where *N* is the total of specimens and n is the rank order of a certain specimen when the specimens are ordered from weakest to strongest.

In order to represent graphically the strength data, the following form of Eq. 5.1 is frequently used:

$$\ln\left(\ln\left(\frac{1}{1-P_f}\right)\right) = m\ln\left(\frac{\sigma}{(\sigma_0)_V}\right) + \ln(V_E) \tag{5.3}$$

Where, $V_E\ (= kV)$ is the effective volume under tension, k is a dimensionless factor and has been identified as a load factor. Eq. 5.3 represents a straight line with slope m when $\ln\left(\ln\left(\frac{1}{1-P_f}\right)\right)$ is plotted against $\ln(\sigma)$. This parameter can then be computed with the use of the least squares method.

The effective volume expression is a function of the Weibull modulus and the geometric parameters of the specimen configuration which possesses a stress distribution. The effective volume can be derived for any configuration from the following equation:

$$V_E = \int_V \left(\frac{\sigma}{\sigma_{\max}}\right)^m dV \tag{5.4}$$

Similarly, the effective surface area can be derived for any configuration from the following equation:

$$A_E = \int_A \left(\frac{\sigma}{\sigma_{\max}}\right)^m dA \tag{5.5}$$

Where, σ is an appropriate expression for the stress distribution and σ_{max} is the maximum stress. In the case when the stress distribution cannot be obtained analytically, the effective volume/ surface area can then be computed numerically. When the strengths of two different specimen configurations of the same material

are to be compared, the following expression will be effectively used. In such case equal failure probabilities are substituted in Eq. 5.3:

$$\frac{\sigma_1}{\sigma_2} = \left(\frac{V_{E2}}{V_{E1}} \right)^{1/m} \tag{5.6}$$

The volume-based Weibull analysis is used when the failure initiating flaws exist in the bulk of the material as well as at the surface, conversely, when failure mainly occurs due to surface flaws, then the area Weibull analysis can better describe the strength distribution. In this case the relationship which corresponds to Eq. 5.6 is

$$\frac{\sigma_1}{\sigma_2} = \left(\frac{A_{E2}}{A_{E1}} \right)^{1/m} \tag{5.7}$$

Where, σ_1, σ_2 are the mean strength of the specimen type 1 and 2; V_{E1}, V_{E2} are effective volumes of the specimen type 1 and 2; A_{E1}, A_{E2} are effective surfaces of the specimen type 1 and 2, respectively(Quinn 2003a, b).

5.3 Weibull Effective Volume and Surface Area for Bimodular Material

In order to show the strength scaling from one loading configuration to another, the present work deals with the bi-modular beam of circular cross-section with different flexural loading configurations. Figs. 5.1 to 5.5 represent respectively the four-point general, four point ¼ point loading, four point 1/3 point loading, three-

point general and uniform bending flexural specimen as corresponding to the location of loading configurations along with its Cartesian X-Y coordinate system.

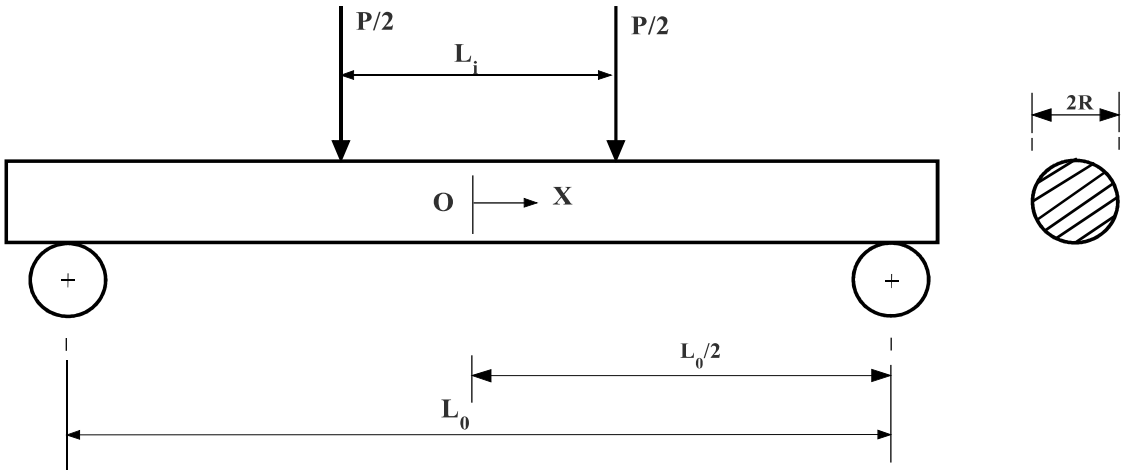

Fig. 5.1 Four-point general flexure specimen

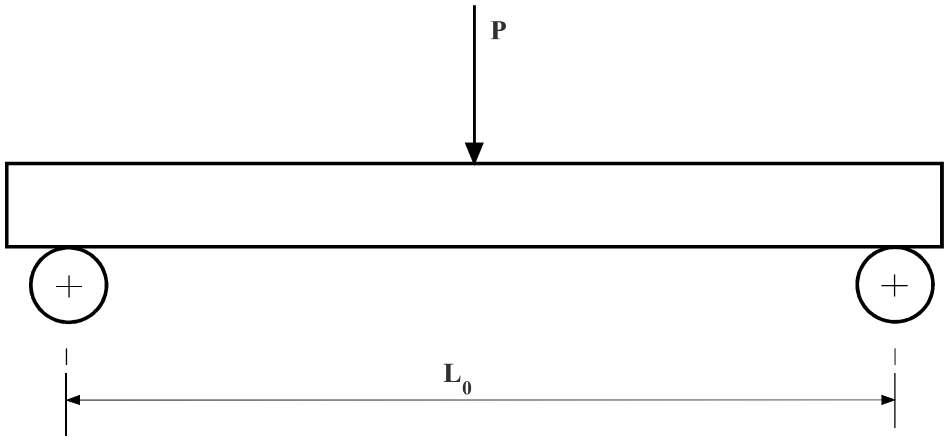

Fig. 5.2 Three-point flexure specimen

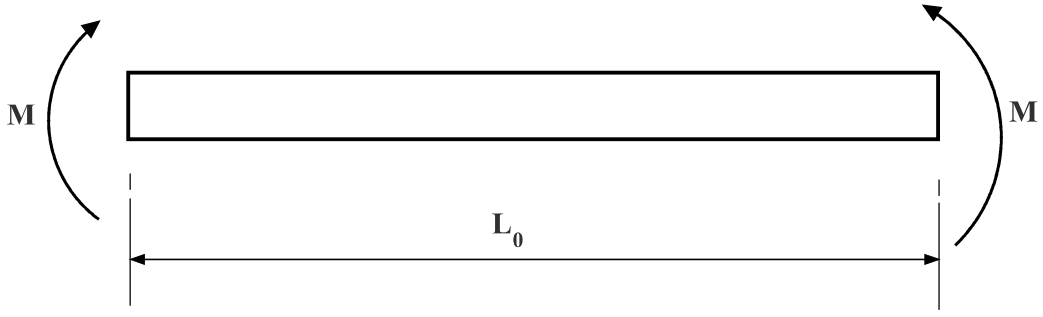

Fig. 5.3 Beam subjected to uniform bending

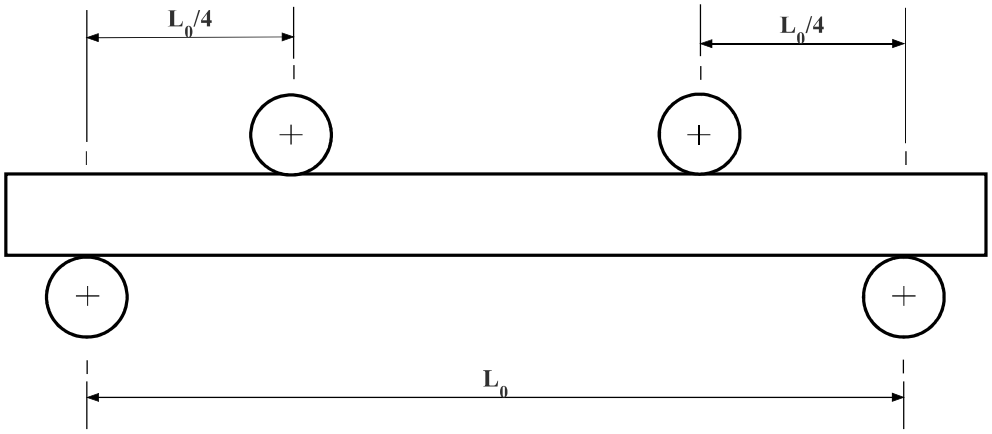

Fig. 5.4 Four-point ¼ point flexure specimen

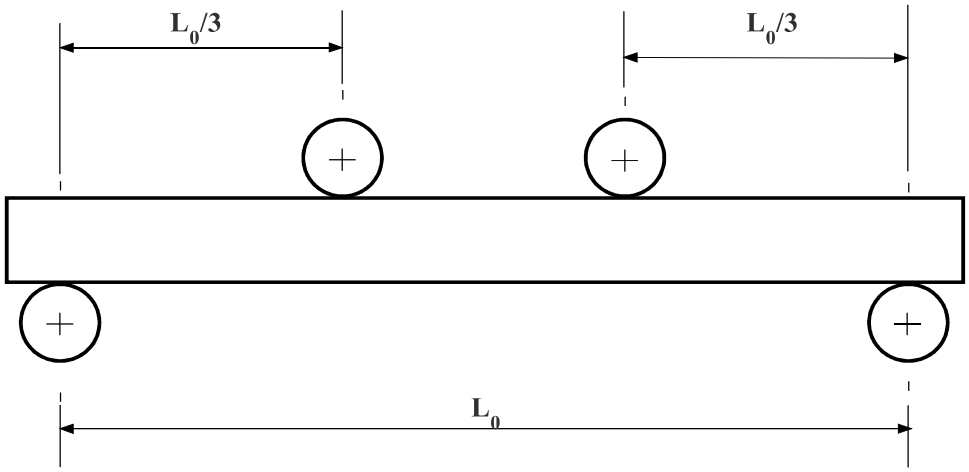

Fig. 5.5 Four-point 1/3 point flexure specimen

The notation x represents the longitudinal coordinate of the flexural beam from the central half-length of each specimen. However, in the present analysis, as the specimen cross section is circular, the cylindrical $r - \phi$ coordinate transformation as delineated in Fig. 5.6 has been referred for deriving Weibull effective volume and effective surface area expressions.

In order to derive the expression for effective volume, effective surface and thereafter strength scaling factor, the following cross-section of the cylindrical beam has been considered, Fig. 5.6. In this figure, δ is the shift of the neutral axis from the centroidal axis of the beam and it is evaluated by force balance at any plane perpendicular to the neutral axis; R is radius of circular cross-section of the cylindrical specimen. At any plane the force balance equation is given by:

$$\int_A \sigma dA = 0 \tag{5.8}$$

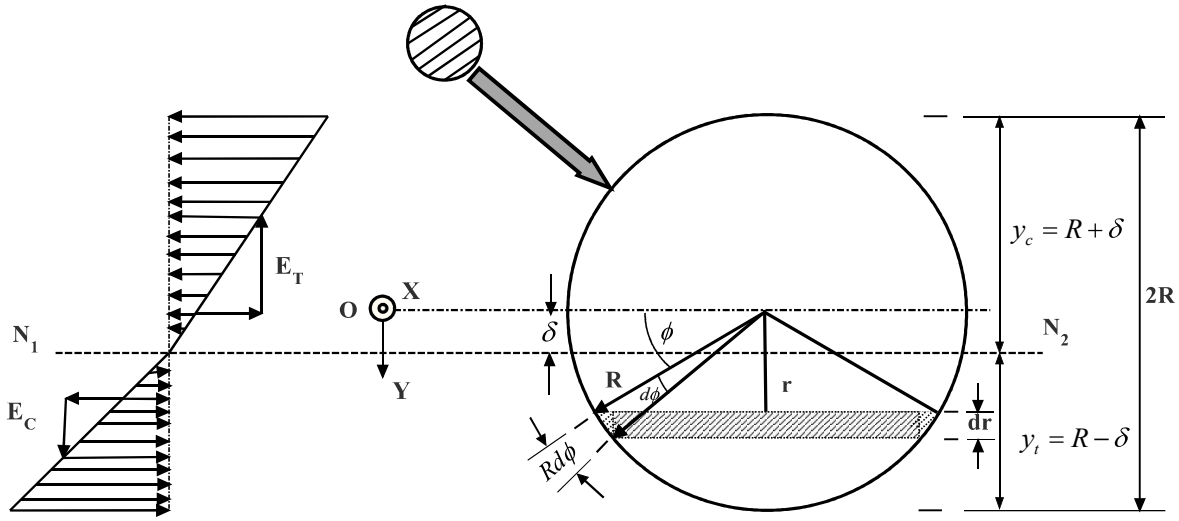

Fig. 5.6 Cylinder cross-section for the effective volume and surface analyses. For the effective volume, the material in the shaded zone is integrated over the cross-section. For the effective surface analysis, the surface length $dS = Rd\phi$ is integrated over the periphery.

Where, the elemental area at a distance r from the centroidal axis is given by

$$dA = 2\sqrt{R^2 - r^2}\,dr \tag{5.9}$$

Now, the stress at a point in the tensile and compressive region is given, respectively, by

$$\sigma_T = \frac{E_T(r-\delta)}{\rho} \tag{5.10}$$

and

$$\sigma_C = \frac{E_C(r+\delta)}{\rho} \tag{5.11}$$

where, ρ is the radius of curvature of the beam.

Using Eq 5.9-5.11 in Eq 5.8 and simplifying, we have the following expression in terms of δ as

$$\frac{E_T}{E_C}\int_{\delta}^{R}(r-\delta)\sqrt{R^2-r^2}\,dr = \int_{-\delta}^{R}(r+\delta)\sqrt{R^2-r^2}\,dr$$

After substituting E_T/E_C by α, one may have

$$\alpha I_1 = I_2 \tag{5.12}$$

Where,

$$I_1 = \int_{\delta}^{R}(r-\delta)\sqrt{R^2-r^2}\,dr$$

$$I_2 = \int_{-\delta}^{R}(r+\delta)\sqrt{R^2-r^2}\,dr$$

$$I_1 = \int_{\delta}^{R} (r-\delta)\sqrt{R^2 - r^2}\, dr$$

$$I_2 = \int_{-\delta}^{R} (r+\delta)\sqrt{R^2 - r^2}\, dr$$

Solutions for I_1 and I_2 can be sought after some manipulations in the following way

$$I_1 = \int_{\delta}^{R} (r-\delta)\sqrt{R^2 - r^2}\, dr$$

$$= \frac{1}{2}\left[\int_{\delta}^{R} 2r\sqrt{R^2 - r^2}\, dr - 2\delta\int_{\delta}^{R}\sqrt{R^2 - r^2}\, dr\right]$$

$$= \frac{1}{2}\left[\frac{2}{3}\left[\left(R^2-\delta^2\right)^{\frac{3}{2}}\right] - 2\delta R^2\int_{\delta}^{R}\sqrt{1-\frac{r^2}{R^2}}\,\frac{dr}{R}\right]$$

$$= \frac{1}{2}\left[\frac{2}{3}\left[\left(R^2-\delta^2\right)^{\frac{3}{2}}\right] - \delta R^2\left[\left(\frac{\pi}{2} - \sin^{-1}\left(\frac{\delta}{R}\right)\right) - \left(\frac{\delta}{R}.\sqrt{1-\left(\frac{\delta}{R}\right)^2}\right)\right]\right]$$

In a similar way,

$$I_2 = \frac{1}{2}\left[\frac{2}{3}\left[\left(R^2-\delta^2\right)^{\frac{3}{2}}\right] + \delta R^2\left[\left(\frac{\pi}{2} + \sin^{-1}\left(\frac{\delta}{R}\right)\right) + \left(\frac{\delta}{R}.\sqrt{1-\left(\frac{\delta}{R}\right)^2}\right)\right]\right]$$

Now, putting the expressions of I_1 and I_2 in Eq 5.12, we have

$$\frac{\alpha}{2}\left[\frac{2}{3}\left[\left(R^2-\delta^2\right)^{\frac{3}{2}}\right] - \delta R^2\left[\left(\frac{\pi}{2} - \sin^{-1}\left(\frac{\delta}{R}\right)\right) - \left(\frac{\delta}{R}.\sqrt{1-\left(\frac{\delta}{R}\right)^2}\right)\right]\right] =$$

$$\frac{1}{2}\left[\frac{2}{3}\left[\left(R^2-\delta^2\right)^{\frac{3}{2}}\right] + \delta R^2\left[\left(\frac{\pi}{2} + \sin^{-1}\left(\frac{\delta}{R}\right)\right) + \left(\frac{\delta}{R}.\sqrt{1-\left(\frac{\delta}{R}\right)^2}\right)\right]\right]$$

$$\left[(\alpha-1)\left[2\left[\left(1-\frac{\delta^2}{R^2}\right)^{\frac{3}{2}}\right] + 3\frac{\delta}{R}\left[\left(\sin^{-1}\left(\frac{\delta}{R}\right)\right) + \left(\frac{\delta}{R}.\sqrt{1-\left(\frac{\delta}{R}\right)^2}\right)\right]\right] - (\alpha+1)\left[3\frac{\delta}{R}\left(\frac{\pi}{2}\right)\right]\right] = 0$$

Let's $\frac{\delta}{R} = \xi$

So,

$$(\alpha-1)\left[2\left[\left(1-\xi^2\right)^{\frac{3}{2}}\right]+3\beta\left[\left(\sin^{-1}(\xi)\right)+\left(\beta.\sqrt{1-(\xi)^2}\right)\right]\right]-(\alpha+1)\left[3\xi\left(\frac{\pi}{2}\right)\right]=0$$

$$2\left(1-\xi^2\right)^{\frac{3}{2}}+3\beta\left(\sin^{-1}(\xi)\right)+3\beta^2.\sqrt{1-(\xi)^2}-\frac{(\alpha+1)}{(\alpha-1)}\left(\frac{3\pi}{2}\right)\xi=0 \qquad (5.13)$$

Here, the shift of the neutral axis is a function of the specimen dimension as well as the E_T/E_C ratio. Thus in order to evaluate the shift, the specimen dimensions must be provided. In the present analysis, the specimen dimensions have been taken from the report by Price (Price 1976). After solving the above equation using Newton-Raphson method, results have been plotted in Fig. 5.7 for the dimensionless ratio of neutral axis shift to radius of the cross-section of the beam over a range of E_T/E_C ratio. This figure reflects that with increase in E_T/E_C ratio, the shift of the neutral axis decrease in a non-linear way.

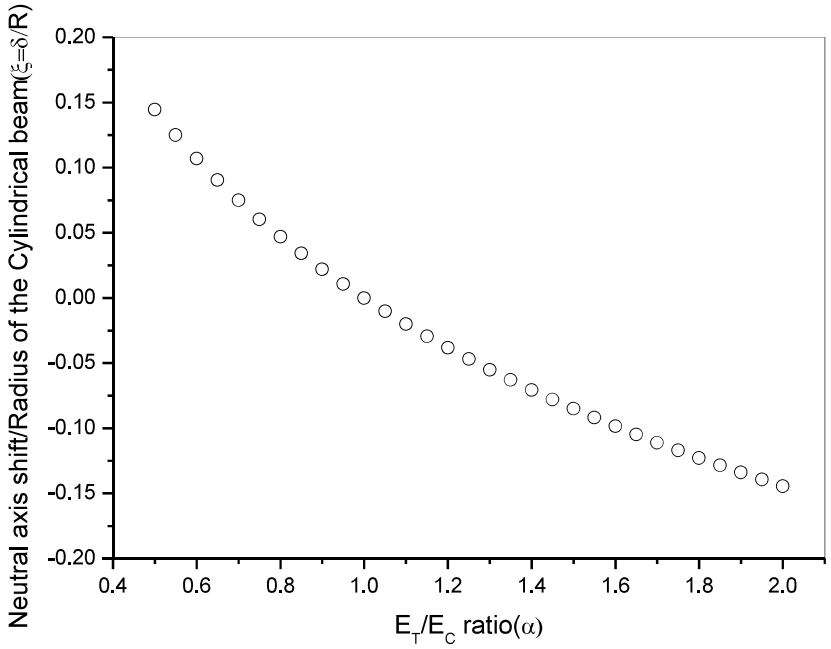

Fig. 5.7 Ratio of Neutral axis shift to radius of circular x-section of the beam (ξ) for a range of E_T/E_C (α)

After evaluating the neutral axis shift, the stress distribution at a point in the cylindrical specimen may be determined from the equation of moment balance about the axis of the specimen. The moment balance equation can be written as

$$\int_{A_t} (\sigma_T dA) \times (r - \delta) + \int_{A_c} (\sigma_C dA) \times (r + \delta) = M \qquad (5.14)$$

Substituting Eqs. (5.9-5.11) in Eq. (5.14), we get

$$\int_{\delta}^{R} \frac{E_t}{\rho} (r - \delta)^2 \, 2\sqrt{R^2 - r^2}\, dr + \int_{\delta}^{-R} \frac{E_c}{\rho} (r + \delta)^2 \, 2\sqrt{R^2 - r^2}\, dr = M$$

After carrying out the integration and on simplification, the above equation turns out to be

$$\frac{E_T R^4}{4\rho} \left[\begin{array}{l} \left(\frac{\pi}{2} - \sin^{-1}\xi + x\left(1-\xi^2\right)^{\frac{3}{2}} - \xi^3\left(1-\xi^2\right)^{\frac{1}{2}} \right) \\ +4\xi^2 \left(\frac{\pi}{2} - \sin^{-1}(\xi) - \xi.\sqrt{1-\xi^2} \right) - \frac{32}{3}\xi\left(1-\xi^2\right)^{\frac{3}{2}} \end{array} \right] +$$

$$\frac{E_C R^4}{4\rho} \left[\begin{array}{l} \left(\frac{\pi}{2} + \sin^{-1}\xi - \xi\left(1-\xi^2\right)^{\frac{3}{2}} + \xi^3\left(1-\xi^2\right)^{\frac{1}{2}} \right) \\ +4\xi^2 \left(\frac{\pi}{2} + \sin^{-1}\xi + \xi\sqrt{1-\xi^2} \right) + \frac{32}{3}\xi\left(1-\xi^2\right)^{\frac{3}{2}} \end{array} \right] = M$$

Now, let us substitute $\xi = \sin\theta$ in the above equation, we obtain

$$\frac{E_T R^4}{4\rho} \left(\left(\frac{\pi}{2} - \theta \right) + \frac{\sin 4\theta}{4} + 4\sin^2\theta \left(\frac{\pi}{2} - \theta - \sin\theta\cos\theta \right) - \frac{32}{3}\sin\theta\cos^3\theta \right) +$$

$$\frac{E_C R^4}{4\rho}\left(\left(\frac{\pi}{2}+\theta\right)-\frac{\sin 4\theta}{4}+4\sin^2\theta\left(\frac{\pi}{2}+\theta+\sin\theta\cos\theta\right)+\frac{32}{3}\sin\theta\cos^3\theta\right)=M$$

Substitution of E_T/E_C by α and $\frac{E_T}{\rho}$ by $\frac{\sigma_T}{(r-\delta)}$ from Eq. 5.10, some treatment yields

$$\frac{\sigma_T R^4}{4(r-\delta)}\{\frac{\pi}{2}\left(1+\frac{1}{\alpha}\right)+\theta\left(-1+\frac{1}{\alpha}\right)+\frac{\sin 4\theta}{4}\left(1-\frac{1}{\alpha}\right)+4\sin^2\theta\left(\frac{\pi}{2}\left(1+\frac{1}{\alpha}\right)\right)+$$

$$(\theta+\sin\theta\cos\theta)\left(-1+\frac{1}{\alpha}\right)+\frac{32}{3}\sin\theta\cos^3\theta\left(-1+\frac{1}{\alpha}\right)\}=M$$

The above equation may also be represented in the form

$$\sigma_T=\frac{4M\left(r-\delta\right)}{R^4 f(\theta,\alpha)} \tag{5.15}$$

Where,

$$f\left(\alpha,\theta\right)=\frac{\pi}{2}\left(1+\frac{1}{\alpha}\right)+\theta\left(-1+\frac{1}{\alpha}\right)+\frac{\sin 4\theta}{4}\left(1-\frac{1}{\alpha}\right)+4\sin^2\theta\left(\frac{\pi}{2}\left(1+\frac{1}{\alpha}\right)\right)+$$

$$(\theta+\sin\theta\cos\theta)\left(-1+\frac{1}{\alpha}\right)+\frac{32}{3}\sin\theta\cos^3\theta\left(-1+\frac{1}{\alpha}\right)$$

5.3.1 Effective Volume for Four Point Flexural Beam with Bimodular Property

Now, the expression for $\sigma_{T\max}$ can be written for the Fig. 5.1 as

$$\sigma_{T\max} = \frac{4P\left(\frac{L_o - L_i}{4}\right)(R-\delta)}{R^4 f(\theta,\alpha)} \tag{5.16}$$

Insertion of Eqs. (5.15-5.16) into Eq. (5.4) and subsequent simplification yields

$$V_E = 2\int_{x=0}^{L_0/2}\int_A \left(\frac{\sigma_T}{\sigma_{T\max}}\right)^m dAdx = 2\int_{x=0}^{L_0/2}\int_A \left(\frac{4M(r-\delta)}{P(L_0 - L_i)(R-\delta)}\right)^m dAdx$$

After some manipulations and simplifications, the above equation turns out to be

$$V_E = \frac{16}{(R-\delta)^m}\left[\int_{x=0}^{L_0/2}\left(\frac{M}{P(L_0 - L_i)}\right)^m dx \int_{\delta}^{R}(r-\delta)^m \sqrt{(R^2 - r^2)}dr\right]$$

It is to be noted here that the integration has been performed over the portions of the specimen that are stressed in tension. After carrying out the integration for the first integral expression, one may have the fully closed form solution as derived in Eq 5.17 below while for the second integral one has to go for the numerical method.

$$V_E = \frac{4}{(R-\delta)^m}\left(1 + m\frac{L_i}{L_0}\right)\left(\frac{L_0}{2(m+1)}\right)\int_{r=\delta}^{R}(r-\delta)^m \sqrt{(R^2 - r^2)}dr \tag{5.17}$$

The above integral term can be effectively evaluated with a programming software such as C-Program/Fortran Program as an area under the curve by taking an elemental differential volume integrated over the domain '*r*' varying from δ to

R. Alternatively, the integral term in Eq. 5.17 has been evaluated using Mathematica and the closed form expression has been given as

$$V_E = \frac{\sqrt{\pi} R^{1-m}}{(R-\delta)^m}\left(1+m\frac{L_i}{L_0}\right)\left(\frac{L_0}{2(m+1)}\right)\left[\frac{R\Gamma\left(\frac{1-m}{2}\right)F_1}{\Gamma\left(2+\frac{m}{2}\right)} - \frac{2\Gamma\left(1+\frac{m}{2}\right)\left[\left(\delta^2-R^2\right)F_2+\left(2\delta^2 m+R^2\right)F_3\right]}{\delta m(2+m)\Gamma\left(\frac{3+m}{2}\right)}\right]$$

$$F_1 = Hypergeometric2F1\left[-1-\frac{m}{2},-\frac{m}{2},\frac{1}{2},\frac{d^2}{R^2}\right]$$

$$F_2 = Hypergeometric2F1\left[\frac{1}{2}(-1-m),\frac{1-m}{2},-\frac{1}{2},\frac{d^2}{R^2}\right]$$

$$F_3 = Hypergeometric2F1\left[\frac{1}{2}(-1-m),\frac{1-m}{2},\frac{1}{2},\frac{d^2}{R^2}\right]$$

Thus, now we have expression of V_E for the bi-modular cylindrical beam loaded in four point flexure.

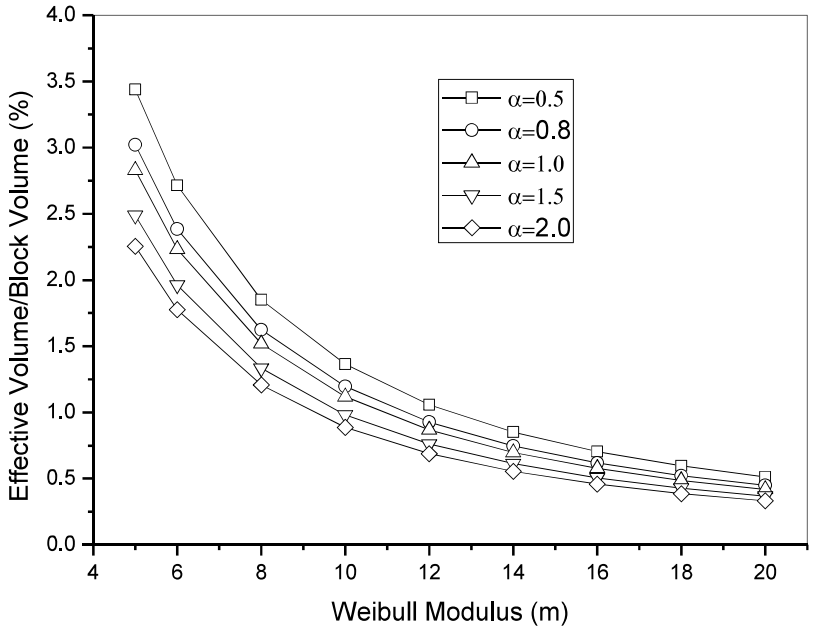

Fig. 5.8 Effect of bi-modularity on effective volume in four-point- ¼ point flexure specimen

For four-point- ¼ point flexure loading (Fig. 5.4), $L_i/L_o = 1/2$ and the Eq. 5.17 leads to

$$V_E = \frac{4}{(R-\delta)^m}\left(1+\frac{m}{2}\right)\left(\frac{L_0}{2(m+1)}\right)\int_{r=\delta}^{R}(r-\delta)^m\sqrt{(R^2-r^2)}dr \qquad (5.18)$$

Similarly, for four-point-1/3 point flexure loading (Fig. 5.5), $L_i/L_o = 1/3$, and the equation for V_E for this case becomes

$$V_E = \frac{4}{(R-\delta)^m}\left(1+\frac{m}{3}\right)\left(\frac{L_0}{2(m+1)}\right)\int_{r=\delta}^{R}(r-\delta)^m\sqrt{(R^2-r^2)}dr \qquad (5.19)$$

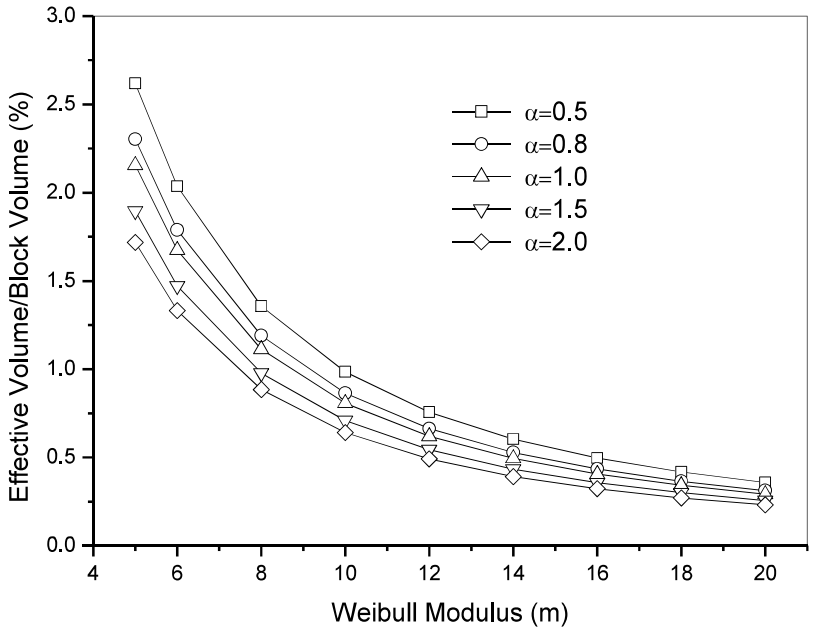

Fig. 5.9 Effect of bi-modularity on effective volume in four-point-1/3 point flexure specimen.

In a similar way, for three point flexure loading, $L_i/L_o = 0$ and the Eq. 5.17 turns out to be

$$V_E = \frac{4}{(R-\delta)^m}\left(\frac{L_0}{2(m+1)}\right)\int_{r=\delta}^{R}(r-\delta)^m\sqrt{(R^2-r^2)}dr \qquad (5.20)$$

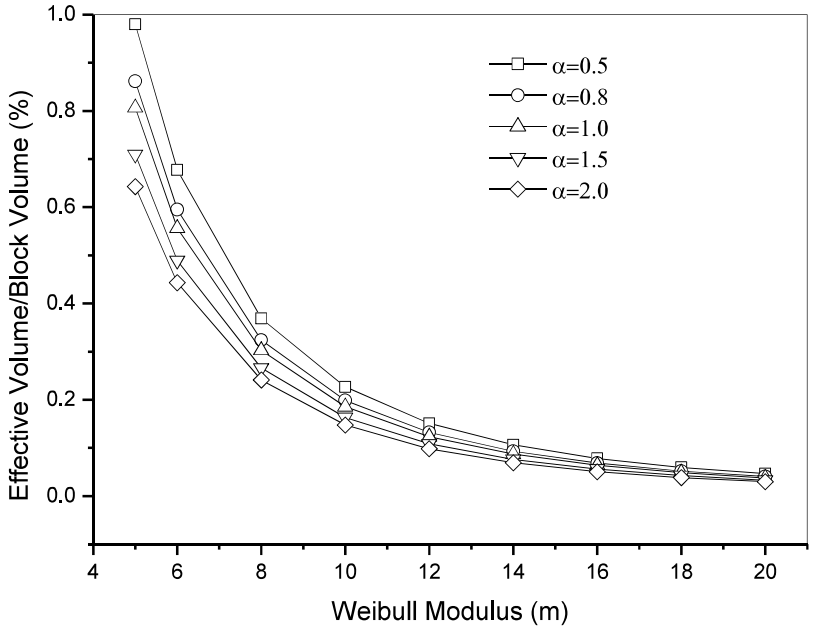

Fig. 5.10 Effect of bi-modularity on effective volume in three point bend specimen

5.3.2 *Effective Volume for Beam Subjected to Uniform Bending with Bimodular property*

Approaching in a similar way like the 4-point bend specimen, now, the expression of σ_{Tmax} in case of beam subjected to uniform bending, (Fig. 5.3) becomes

$$\sigma_{T\max} = \frac{4M(R-\delta)}{R^4 f(\theta,\alpha)} \qquad (5.21)$$

Inserting Eq. 5.15 and Eq. 5.21 into Eq. 5.4 yields

$$V_E = \int_V\left(\frac{\sigma_T}{\sigma_{T\max}}\right)^m dV = 2\int_{x=0}^{L_0/2}\int_A\left(\frac{(r-\delta)}{(R-\delta)}\right)^m dAdx$$

$$= L_o \left(\frac{1}{(R-\delta)} \right)^m \int_{r=\delta}^{R} (r-\delta)^m \, 2\sqrt{(R^2 - r^2)} dr \qquad (5.22)$$

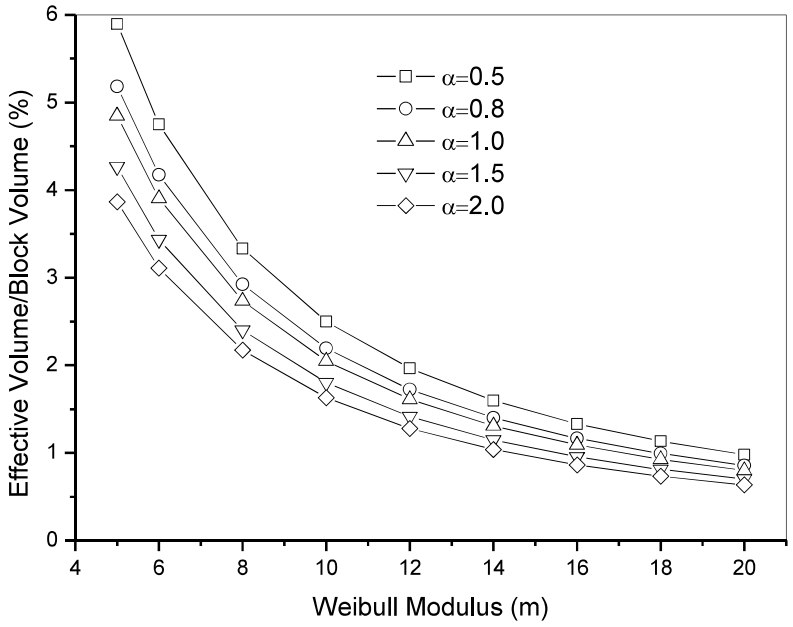

Fig. 5.11 Effect of bi-modularity on effective volume in uniform bending specimen

After carrying out the second integration numerically, and combining with the first part of the Eq. 5.18-5.20 and Eq 5.22, the effective volumes of the four point and three point flexure specimens for different loading configurations as well as for the uniform bending specimen, have been plotted as a function of the Weibull modulus, m, for different E_T/E_C ratio, Figs. 5.8 - 5.11. The effective volume is a function of the specimen shape and dimension as well as the Weibull modulus. From all the four figures above it is reflected that the ratio of E_T/E_C has a significant effect on effective volume; also the lowest E_T/E_C configuration has the largest effective volume and with the increase in the Weibull modulus value there is asymptotic decrease in the value of the effective volume. Also with the

increase in Weibull modulus value, it is observed that the differences in the effective volume values reduce gradually for the range of E_T/E_C. Table 5.1 provides a comparison of the results obtained for V_E *and* A_E for all four different kinds of flexural loading from the present formulation with the results obtained from the expressions developed in earlier literature by Quinn(Quinn 2003a) with unimodular assumption.

Table 5.1 Comparison of the results (V_E and A_E) obtained from the newly developed semi-analytical expressions in this chapter with the analytical expression developed by Quinn (Quinn 2003a); Unimodular beam with *Weibull Modulus m = 10, R = 3.2 mm and* L_0 *= 51 mm.*

Beam Configuration and Loading	V_E as per (Quinn 2003a)(mm^3)	V_E, Present Method (mm^3)	A_E as per (Quinn 2003a)(mm^2)	A_E, Present Method (mm^2)
Four-point ¼ point flexure specimen	18.35247	18.347218	68.82142	68.8189
Four-point 1/3 point flexure specimen	13.2546	13.2508	49.7047	49.7025
Three point flexure	3.058692	3.0579	11.47024	11.4698
Uniform bending	33.64643	33.6366	126.1726	126.1679

The qualitative and quantitative agreement of the results justifies the appropriateness of the present work towards the more generalized bimodular formulations. However, elaborate experimentation for each category of loading can be considered as a future work for such bimodular materials like graphite, for which these expressions become the impetus of further study. As a matter of fact, bimodular experimentations are not only rare in literature, but also if their readings are not properly calibrated, they shall be much more prone to errors in

predicting the strength scaling from one specimen size to another and from one loading configuration to another.

Moreover, it should be noted here that in case of tubular and C-ring specimens, similar kinds of qualitative results were obtained by the previous researchers (Jadaan et al. 1991; Shelleman et al. 1991; Duffy et al. 2005). The reason for lowest E_T/E_C configuration having the largest effective volume is that the specimen in this case possesses the largest volume which is stressed in tension.

5.3.3 Effective Surface Area for Four Point Flexural Beam with Bimodular Property

After putting the Eq. 5.15-5.16 into Eq. 5.5, one may have

$$A_E = \int_A \left(\frac{\frac{4My}{R^4 f(\theta,\alpha)}}{\frac{4P\left(\left(L_o - L_i\right)/4\right)(R-\delta)}{R^4 f(\theta,\alpha)}} \right)^m dA$$

$$= 2\int_0^{\frac{L_o}{2}} \int_{\sin^{-1}\frac{\delta}{R}}^{\frac{\pi}{2}} \left(\frac{4M}{P\left(L_o - L_i\right)} \right)^m dx \frac{\left(R\sin\phi - \delta\right)^m}{\left(R-\delta\right)^m} Rd\phi$$

After simplification, one gets

$$A_E = \frac{2R}{\left(R-\delta\right)^m} \left(1 + m\frac{L_i}{L_0}\right) \left(\frac{L_0}{2(m+1)}\right) \int_{\sin^{-1}\frac{\delta}{R}}^{\frac{\pi}{2}} \left(R\sin\phi - \delta\right)^m d\phi \qquad (5.23)$$

For four-point- ¼ point flexure loading, $L_i/L_o = 1/2$ and Eq. 5.23 leads to

$$A_E = \frac{2R}{(R-\delta)^m}\left(1+\frac{m}{2}\right)\left(\frac{L_0}{2(m+1)}\right)\int_{\sin^{-1}\frac{\delta}{R}}^{\frac{\pi}{2}} (R\sin\phi-\delta)^m\, d\phi \qquad (5.24)$$

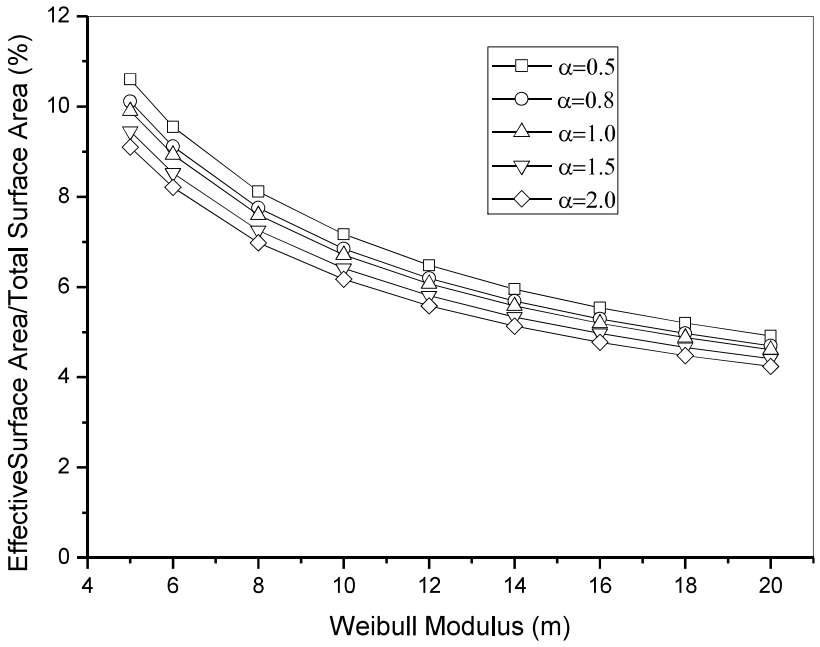

Fig. 5.12 Effect of bi-modularity on effective surface in four-point- ¼ point flexure specimen

For four-point- 1/3 point flexure loading, $L_i/L_o = 1/3$ and the above equation leads to

$$A_E = \frac{2R}{(R-\delta)^m}\left(1+\frac{m}{3}\right)\left(\frac{L_0}{2(m+1)}\right)\int_{\sin^{-1}\frac{\delta}{R}}^{\frac{\pi}{2}} (R\sin\phi-\delta)^m\, d\phi \qquad (5.25)$$

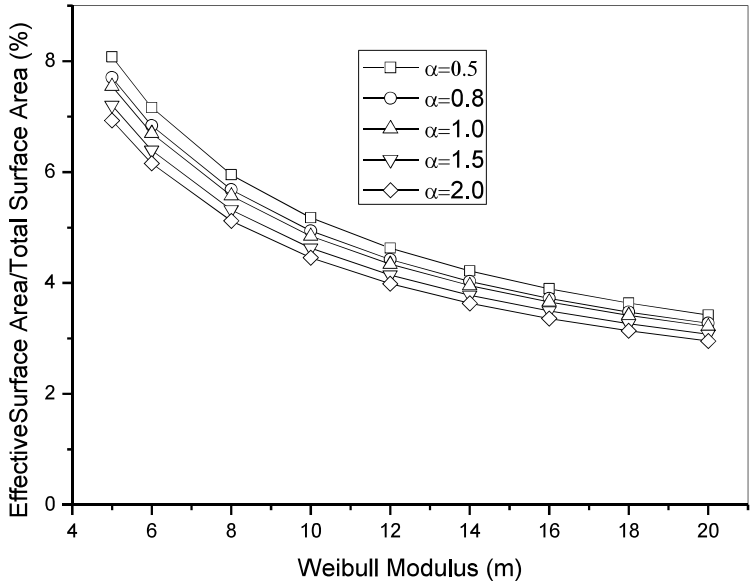

Fig. 5.13 Effect of bi-modularity on effective surface in four-point- 1/3 point flexure specimen

For three point flexural loading, $L_i/L_o = 0$ and the Eq 5.23 leads to

$$A_E = \frac{2R}{(R-\delta)^m}\left(\frac{L_0}{2(m+1)}\right)\int_{\sin^{-1}\frac{\delta}{R}}^{\frac{\pi}{2}} (R\sin\phi - \delta)^m \, d\phi \qquad (5.26)$$

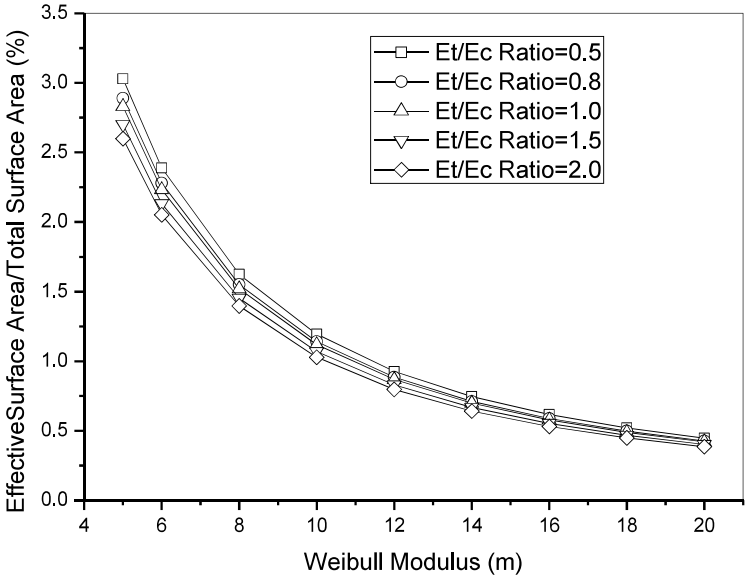

Fig. 5.14 Effect of bi-modularity on effective surface in three point bend specimen

5.3.4 Effective Surface Area for Beam Subjected to Uniform Bending with Bimodular property

Inserting Eq. 5.15 and Eq. 5.21 into Eq. 5.5 yields

$$A_E = \int_A \left(\frac{\frac{4M(r-\delta)}{R^4 f(\theta,\alpha)}}{\frac{4M(R-\delta)}{R^4 f(\theta,\alpha)}} \right)^m dA$$

Simplification yields

$$A_E = \frac{2R}{(R-\delta)^m} \frac{L_o}{2} \int_{\sin^{-1}\frac{\delta}{R}}^{\frac{\pi}{2}} (R\sin\phi - \delta)^m \, d\phi \tag{5.27}$$

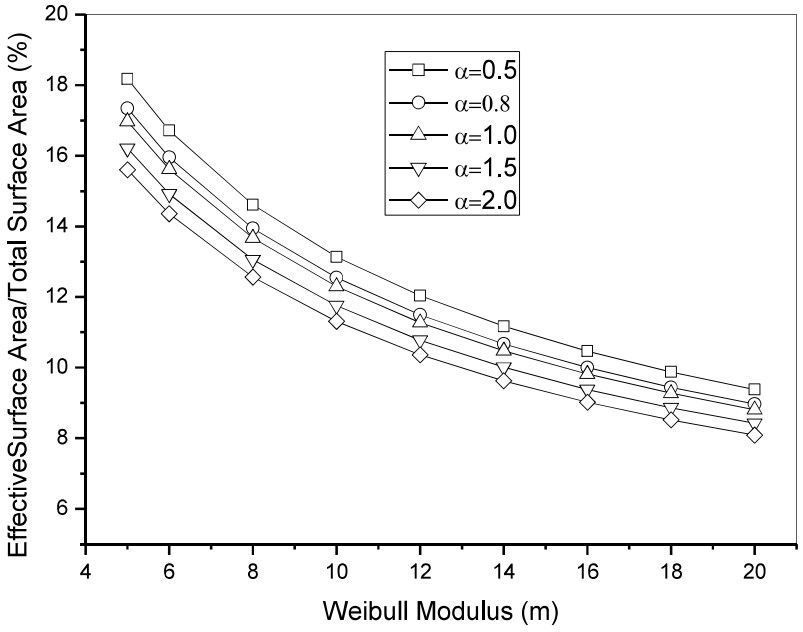

Fig. 5.15 Effect of bi-modularity on effective surface in uniform bending,

Approaching in a similar way, after carrying out the second integration numerically, and combining with the first part of the Eq. 5.24 – 5.27, the effective

surface areas of the four point and three point flexure specimens along with the beam in uniform bending for different loading configurations, have been plotted as a function of the Weibull modulus, m, for different E_T/E_C ratio, Fig. 5.12 – Fig. 5.15. Like effective volume, here also, from all the four figures above it is revealed that the ratio of E_T/E_C has a significant effect on effective surface; as well the lowest E_T/E_C configuration has the largest effective surface and with the increase in the Weibull modulus value there is asymptotic decrease in the value of the effective surface.

Table 5.2 Final expressions of the *effective volume* for cylindrical beam loaded in flexure

(a) Effective Volume (Integral Form Expression)

Four point general	$V_E = \frac{4}{(R-\delta)^m}\left(1+m\frac{L_i}{L_0}\right)\left(\frac{L_0}{2(m+1)}\right)\int_{r=\delta}^{R}(r-\delta)^m\sqrt{(R^2-r^2)}dr$
Four-point ¼ point flexure specimen	$V_E = \frac{4}{(R-\delta)^m}\left(1+\frac{m}{2}\right)\left(\frac{L_0}{2(m+1)}\right)\int_{r=\delta}^{R}(r-\delta)^m\sqrt{(R^2-r^2)}dr$
Four-point 1/3 point flexure specimen	$V_E = \frac{4}{(R-\delta)^m}\left(1+\frac{m}{3}\right)\left(\frac{L_0}{2(m+1)}\right)\int_{r=\delta}^{R}(r-\delta)^m\sqrt{(R^2-r^2)}dr$
Three point flexure	$V_E = \frac{4}{(R-\delta)^m}\left(\frac{L_0}{2(m+1)}\right)\int_{r=\delta}^{R}(r-\delta)^m\sqrt{(R^2-r^2)}dr$
Uniform bending	$V_E = L_o\left(\frac{1}{(R-\delta)}\right)^m\int_{r=\delta}^{R}(r-\delta)^m 2\sqrt{(R^2-r^2)}dr$

(b) Effective Volume (Closed Form Solution)

Four point general	$V_E = \frac{\sqrt{\pi} R^{1-m}}{(R-\delta)^m}\left(1+m\frac{L_i}{L_0}\right)\left(\frac{L_0}{2(m+1)}\right)\left[\frac{R\Gamma\left(\frac{1-m}{2}\right)F_1}{\Gamma\left(2+\frac{m}{2}\right)} - \frac{2\Gamma\left(1+\frac{m}{2}\right)\left[\left(\delta^2-R^2\right)F_2+\left(2\delta^2 m+R^2\right)F_3\right]}{\delta m(2+m)\Gamma\left(\frac{3+m}{2}\right)}\right]$
Four-point ¼ point flexure specimen	$V_E = \frac{\sqrt{\pi} R^{1-m}}{(R-\delta)^m}\left(1+\frac{m}{2}\right)\left(\frac{L_0}{2(m+1)}\right)\left[\frac{R\Gamma\left(\frac{1-m}{2}\right)F_1}{\Gamma\left(2+\frac{m}{2}\right)} - \frac{2\Gamma\left(1+\frac{m}{2}\right)\left[\left(\delta^2-R^2\right)F_2+\left(2\delta^2 m+R^2\right)F_3\right]}{\delta m(2+m)\Gamma\left(\frac{3+m}{2}\right)}\right]$
Four-point 1/3 point flexure specimen	$V_E = \frac{\sqrt{\pi} R^{1-m}}{(R-\delta)^m}\left(1+\frac{m}{3}\right)\left(\frac{L_0}{2(m+1)}\right)\left[\frac{R\Gamma\left(\frac{1-m}{2}\right)F_1}{\Gamma\left(2+\frac{m}{2}\right)} - \frac{2\Gamma\left(1+\frac{m}{2}\right)\left[\left(\delta^2-R^2\right)F_2+\left(2\delta^2 m+R^2\right)F_3\right]}{\delta m(2+m)\Gamma\left(\frac{3+m}{2}\right)}\right]$
Three point flexure	$V_E = \frac{\sqrt{\pi} R^{1-m}}{(R-\delta)^m}\left(\frac{L_0}{2(m+1)}\right)\left[\frac{R\Gamma\left(\frac{1-m}{2}\right)F_1}{\Gamma\left(2+\frac{m}{2}\right)} - \frac{2\Gamma\left(1+\frac{m}{2}\right)\left[\left(\delta^2-R^2\right)F_2+\left(2\delta^2 m+R^2\right)F_3\right]}{\delta m(2+m)\Gamma\left(\frac{3+m}{2}\right)}\right]$
Uniform bending	$V_E = \frac{L_o}{2}\left(\frac{1}{(R-\delta)}\right)^m \sqrt{\pi} R^{1-m}\left[\frac{R\Gamma\left(\frac{1-m}{2}\right)F_1}{\Gamma\left(2+\frac{m}{2}\right)} - \frac{2\Gamma\left(1+\frac{m}{2}\right)\left[\left(\delta^2-R^2\right)F_2+\left(2\delta^2 m+R^2\right)F_3\right]}{\delta m(2+m)\Gamma\left(\frac{3+m}{2}\right)}\right]$

Table 5.3 Final expressions of the *effective surface* for cylindrical beams loaded in flexure

Four point general	$A_E = \frac{2R}{(R-\delta)^m}\left(1+m\frac{L_i}{L_0}\right)\left(\frac{L_0}{2(m+1)}\right)\int_{\sin^{-1}\frac{\delta}{R}}^{\frac{\pi}{2}}(R\sin\phi-\delta)^m\,d\phi$
Four-point ¼ point flexure specimen	$A_E = \frac{2R}{(R-\delta)^m}\left(1+\frac{m}{2}\right)\left(\frac{L_0}{2(m+1)}\right)\int_{\sin^{-1}\frac{\delta}{R}}^{\frac{\pi}{2}}(R\sin\phi-\delta)^m\,d\phi$
Four-point 1/3 point flexure specimen	$A_E = \frac{2R}{(R-\delta)^m}\left(1+\frac{m}{3}\right)\left(\frac{L_0}{2(m+1)}\right)\int_{\sin^{-1}\frac{\delta}{R}}^{\frac{\pi}{2}}(R\sin\phi-\delta)^m\,d\phi$
Three point flexure	$A_E = \frac{2R}{(R-\delta)^m}\left(\frac{L_0}{2(m+1)}\right)\int_{\sin^{-1}\frac{\delta}{R}}^{\frac{\pi}{2}}(R\sin\phi-\delta)^m\,d\phi$
Uniform bending	$A_E = \frac{2R}{(R-\delta)^m}\frac{L_o}{2}\int_{\sin^{-1}\frac{\delta}{R}}^{\frac{\pi}{2}}(R\sin\phi-\delta)^m\,d\phi$

5.4 Strength Scaling

The present section provides strength scaling ratios of flexural cylindrical specimen with bi-modular property for both surface and volume flaw distribution. Strength scaling ratios are derived below for the conversion of strengths among the various flexural loading configurations.

When volume distributed flaws dominate, strength scaling ratio for the four-point 1/3 point flexural strength to the four-point ¼ point flexural strength, is

$$\frac{\sigma_{4pt,1/3}}{\sigma_{4pt,1/4}} = \left(\frac{V_{E,4pt,1/4}}{V_{E,4pt,1/3}}\right)^{1/m} = \left[\frac{\frac{4}{(R_{4pt,1/4}-\delta)^m}\left(1+\frac{m}{2}\right)\left(\frac{L_{4pt,1/4}}{2(m+1)}\right)\int_{r=\delta}^{R}(r-\delta)^m\sqrt{(R_{4pt,1/4}^2-r^2)}dr}{\frac{4}{(R_{4pt,1/3}-\delta)^m}\left(1+\frac{m}{3}\right)\left(\frac{L_{4pt,1/3}}{2(m+1)}\right)\int_{r=\delta}^{R}(r-\delta)^m\sqrt{(R_{4pt,1/3}^2-r^2)}dr}\right]^{1/m} \tag{5.28}$$

Once, the cross-sections are same, and lengths are according to the fixtures size, ISO 14704 and ISO 17565, (ISO 17565 2003; ISO 14704 2008), the strength ratio correspondingly becomes

$$\frac{\sigma_{4\,pt,1/3}}{\sigma_{4\,pt,1/4}} = \left[\frac{2\left(2+m\right)}{\left(3+m\right)}\right]^{1/m} \tag{5.29}$$

In a similar way, when surface distributed flaws dominate, strength scaling depends on effective area of the specimen and the ratio is

$$\frac{\sigma_{4\,pt,1/3}}{\sigma_{4\,pt,1/4}} = \left(\frac{A_{E,4\,pt,1/4}}{A_{E,4\,pt,1/3}}\right)^{1/m} = \left[\frac{\dfrac{2R}{\left(R_{4\,pt,1/4}-\delta\right)^{m}}\left(1+\dfrac{m}{2}\right)\left(\dfrac{L_{4\,pt,1/4}}{2(m+1)}\right)\displaystyle\int_{\sin^{-1}\frac{\delta}{R}}^{\frac{\pi}{2}}\left(R_{4\,pt,1/4}\sin\phi-\delta\right)^{m}d\phi}{\dfrac{2R}{\left(R_{4\,pt,1/3}-\delta\right)^{m}}\left(1+\dfrac{m}{3}\right)\left(\dfrac{L_{4\,pt,1/3}}{2(m+1)}\right)\displaystyle\int_{\sin^{-1}\frac{\delta}{R}}^{\frac{\pi}{2}}\left(R_{4\,pt,1/3}\sin\phi-\delta\right)^{m}d\phi}\right]^{1/m} \tag{5.30}$$

In case of same cross sections and when the lengths are according to the fixtures size mentioned in (ISO 17565 2003; ISO 14704 2008), the above ratio turns out to be

$$\frac{\sigma_{4\,pt,1/3}}{\sigma_{4\,pt,1/4}} = \left[\frac{2\left(2+m\right)}{\left(3+m\right)}\right]^{1/m} \tag{5.31}$$

Therefore, it can be interestingly observed here that the strength scaling ratios for the four-point-1/3 point flexural strength to the four-point-1/4 point flexural

strength are identical, irrespective of the flaw distribution in the specimen provided that the cross-section remains the same. So

$$\frac{\sigma_{4\,pt,1/3}}{\sigma_{4\,pt,1/4}} = \left(\frac{V_{E,4\,pt,1/4}}{V_{E,4\,pt,1/3}}\right)^{1/m} = \left(\frac{A_{E,4\,pt,1/4}}{A_{E,4\,pt,1/3}}\right)^{1/m} = \left[\frac{2(2+m)}{(3+m)}\right]^{1/m} = W_1 \qquad (5.32)$$

Approaching in a similar way, strength scaling ratio for three-point flexural strength to the four-point-1/3 point flexural strength (when cross sections are remaining the same) is

$$\frac{\sigma_{3\,pt}}{\sigma_{4\,pt,1/3}} = \left(\frac{V_{E,4\,pt,1/3}}{V_{E,3\,pt}}\right)^{1/m} = \left(\frac{A_{E,4\,pt,1/3}}{A_{E,3\,pt}}\right)^{1/m} = \left(1+\frac{m}{3}\right)^{1/m} = W_2 \qquad (5.33)$$

Table 5.4 Conversion factor for converting strengths among four-point and three-point flexure specimens having similar dimension but different loading configurations

Weibull Modulus (m)	Conversion factor		
	W_1	W_2	W_3
5	1.118427	1.216729	1.284735
6	1.100642	1.200937	1.259921
7	1.087596	1.187673	1.239698
8	1.077593	1.176343	1.222845
9	1.069668	1.166529	1.208544
10	1.063229	1.157930	1.196231
12	1.053389	1.143530	1.176047
15	1.043311	1.126878	1.153350
20	1.032967	1.107211	1.127378
25	1.026619	1.093456	1.109720
30	1.022325	1.083211	1.096825

Likewise, strength scaling ratio for three-point flexural strengths to the four-point, 1/4 point flexural strengths (when cross sections are remaining the same),

$$\frac{\sigma_{3\,pt}}{\sigma_{4\,pt,1/4}} = \left(\frac{V_{E,4\,pt,1/4}}{V_{E,3\,pt}} \right)^{1/m} = \left(\frac{A_{E,4\,pt,1/4}}{A_{E,3\,pt}} \right)^{1/m} = \left(1 + \frac{m}{2} \right)^{1/m} = W_3 \qquad (5.34)$$

As a ready reference, the strength scaling conversion factors W_1, W_2 and W_3 have been provided for various Weibull modulus in Table 5.4.

5.5 Experimental Validation

High purity machined graphite tensile and compressive specimens of 20 mm gage diameter have been tested as per ASTM C-749 and ASTM C-695 for assessing the bimodular behavior. Gage length of tensile specimen is 80 mm and for compression specimen is 40 mm (ASTM C695-15 2015; ASTM C749 −15 2015). Twenty specimens from each category are tested at room temperature using INSTRON UTM and the results are recorded for assessing the bimodular behaviour. Utmost care has been taken for preparing the specimens as per ASTM standard with reference to surface finish and planeness of the specimens within the tolerance values. A crosshead speed of 0.2 mm/min has been maintained throughout the testing. The tensile Young's Modulus of elasticity E_T = 8.502 GPa and the compressive Young's Modulus of elasticity E_C = 5.618 GPa were evaluated according to ASTM E111 − 04 (Reapproved 2010) below the proportional limit(ASTM E111-04 2010). Modulus of elasticity values are the average value for all twenty specimens tested in each tension and compression. Two size of flexural specimens are tested for flexural loading as shown in Fig. 5.16, conveniently called (i) Large flexural specimen and small flexural specimen of respective dimension 20 mm diameter, length 128 mm and 10 mm diameter,

length 64 mm (specimen made according to ASTM: D7972-14) for different loading conditions (ASTM D7972-14 2014).

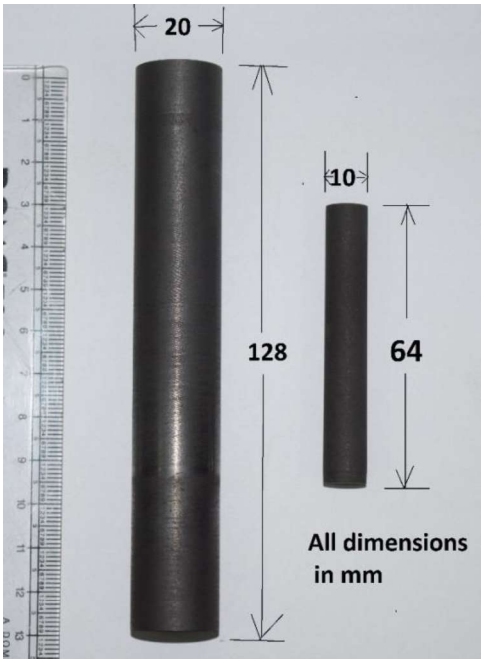

Fig. 5.16 Cylindrical flexural specimen

(a) (b)

Fig. 5.17 Three point flexure assembly for (a) large, (b) small bimodular cylindrical graphite specimens

(a) (b)

Fig. 5.18 Four point 1/3 loading flexure assembly for (a) large, (b) small bimodular cylindrical graphite specimens

(a) (b)

Fig. 5.19 Four point ¼ loading flexure assembly for (a) large, (b) small bimodular cylindrical graphite specimens.

Table 5.5 Cylindrical loading span specifications for flexural specimen

Flexural Loading condition	Size	Outer span (mm)	Inner span (mm)	Specimen Tested
Three point bend specimen	Small	50	0	60
	Large	100	0	60
Four Point Bend 1/3 loading	Small	51	17	60
	Large	102	34	60
Four Point Bend 1/4 loading	Small	50	25	58
	Large	100	50	55

Sixty specimens each were tested for three point bend test, four point bend test 1/3 loading condition and four point bend test 1/4 loading condition as shown in Fig. 5.17-5.19 for every size of specimens. The following **Table 5.5** represents the

support span (outer span) and loading span (inner span) for the different loading conditions.

5.5.1 Evaluation of Weibull Parameters

To evaluate the effective volume and effective surface area and to deal with the probability of failure for a component in a room temperature following ASTM standard, the component or test specimen should be treated as a system. This typical approach to design the structural components with varying complex stress fields encompasses discretizing the component in order to characterize the stress field using finite element solution. Because the component failure may initiate in any of the discrete elements as assume weakest link, it is appropriate to consider a component as a system and utilize system reliability theories. If a component is in series system then failure in one discrete element leads to a sudden catastrophic failure of the whole component. These types of catastrophic failure can be exhibited using the concept of weakest-link theory. Accordingly, one needs a distribution that describes this extreme phenomenon of the sudden failure of the whole component due to the failure of a small weakest link (element). The Weibull distribution with a weakest-link system approach is well-known as Weibull theory (Weibull 1939b).

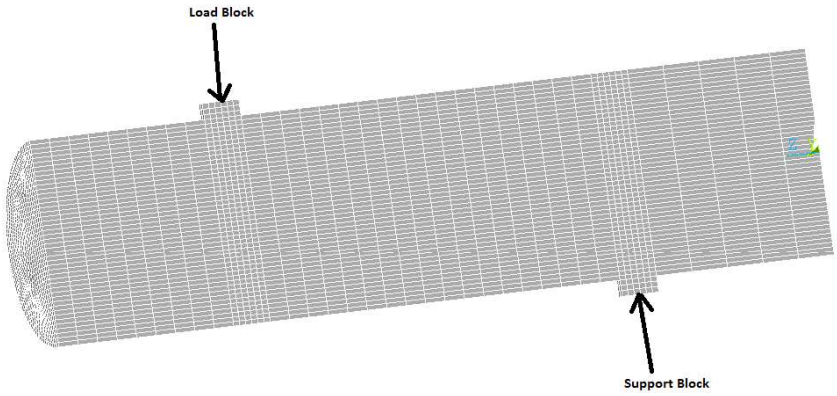

(a)

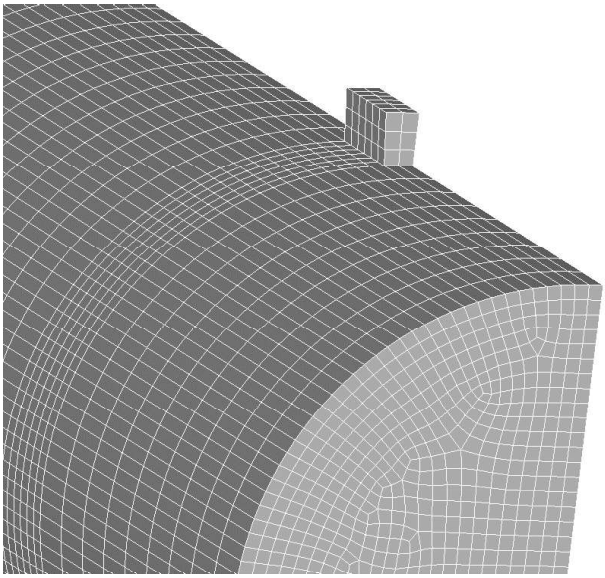

(b)

Fig. 5.20 Quarter symmetry finite element mesh of the cylindrical four-point-flexure 1/3 loading specimen. (a) Overall model with support blocks. (b) Mesh details at the load block.

The quarter symmetric finite element model developed for the flexural specimen is shown in **Fig. 5.20**. The results are finite element mesh sensitive, it has taken rigorous effort to control the mesh to find the results, so it is convenient that the mesh was taken in a similar fashion as taken in(Nemeth et al. 2012), and model built in using ANSYS, Version 14.5 software. The support and load blocks were

modeled for avoiding the stress singularity which directly affect the value of effective volume and effective surface dimensions for flexural tabulated in Table 5.6. The Young's Modulus of elasticity is taken as E_T value as found in experimental results. The Poisson's ratio for both the body, support and load were taken as 0.35, whereas the Modulus of elasticity for support materials has been taken $1/10^{th}$ of E_T value for the high purity graphite. The pressure load on the block was arbitrarily 14.06 N/m^2 (Pa) as taken in(Nemeth et al. 2012, 2013).

Table 5.6 Support and block dimension in formulating finite element model.

Flexural Loading condition	Size	Support block (mm)	Load block (mm)	Span of arc angle, quarter-symmetric (degree)	Width of the block (mm)	Height of the block
Three point bend specimen	Small	1.2	1.2	5	0.44	0.5
	Large	2.4	2.4	5	0.88	1.0
Four Point Bend 1/3 loading	Small	1.2	1.2	5	0.44	0.5
	Large	2.4	2.4	5	0.88	1.0
Four Point Bend 1/4 loading	Small	1.2	1.2	5	0.44	0.5
	Large	2.4	2.4	5	0.88	1.0

The support and load blocks were set to mimic a soft material to help mitigate stress concentrations from hertzian contact. The Weibull plot depicting the probability of failure for three point and four point bend specimen for two loading condition, namely flexural 1/3 loading and flexural ¼ loading condition have been shown in Fig. 5.21 to 5.26 with the aid of best possible fit line using Linear regression (LIN2), biased maximum likelihood estimator (MLE2-B) and unbiased maximum likelihood estimator (MLE2-U) for small and large size specimen using Weibpar (Weibull Distribution Parameter Estimation) version-4.3 and CARES (Ceramics Analysis and Reliability Evaluation of Structures) version-9.3.2.196

Software developed by Connecticut Reserve Technologies, (NASA) USA appropriate quarter symmetric finite element model. The meshing pattern for quarter-symmetric four point 1/3 flexural loading condition for small size specimen dimension is shown in Figure 20. Similar sort of meshing pattern has been developed for other different loading conditions and solved for specific boundary conditions. The finite elements results file has been taken as input file by the CARES software and generate the CARES Natural file which stores the data of stress, strain, displacement, coordinates for each and every nodes for using the data for reliability analysis. Weibpar is the software used in plotting the experimental data with Weibull distribution using weakest link theory. And the Weibull plots for different loading conditions has been shown in Fig. 5.21-5.26.

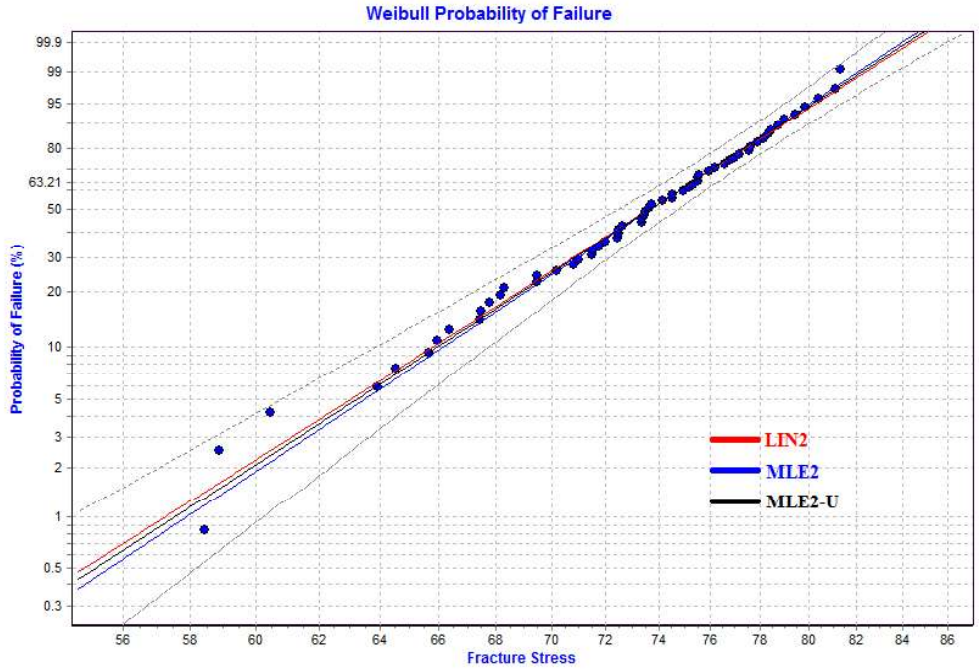

(a)

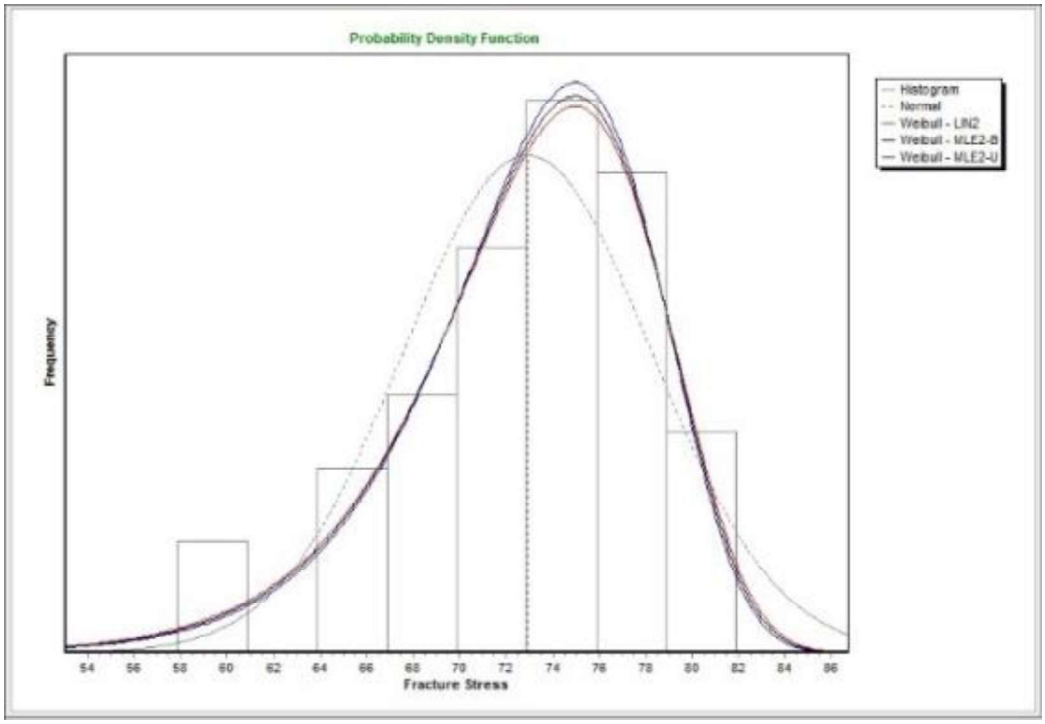

(b)

Fig. 5.21 Weibull plot for small three point bend specimen best fit line for LIN2 (Linear regression with two parameter Weibull distribution), MLE2-B (Biased maximum likelihood estimator with two parameter Weibull distribution) and MLE2-U (Unbiased maximum likelihood estimator with two parameter Weibull distribution parameter Weibull distribution) (b) Weibull PDF and Normal PDF plot and the failure strength data plot in histogram form

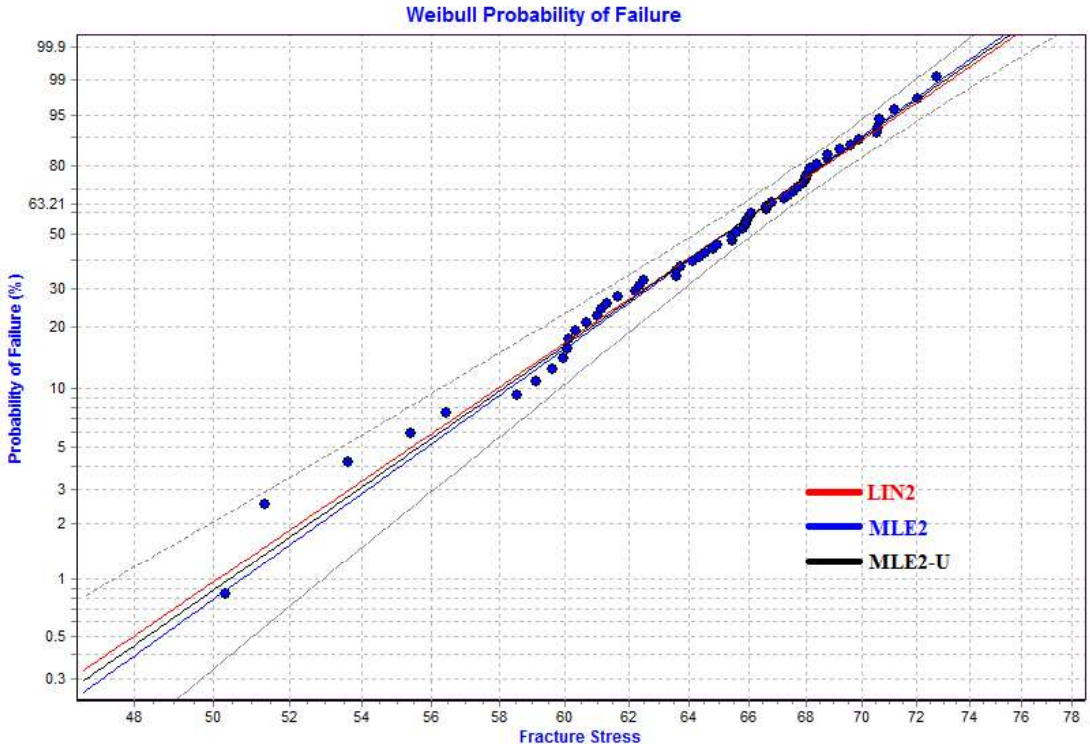

(a)

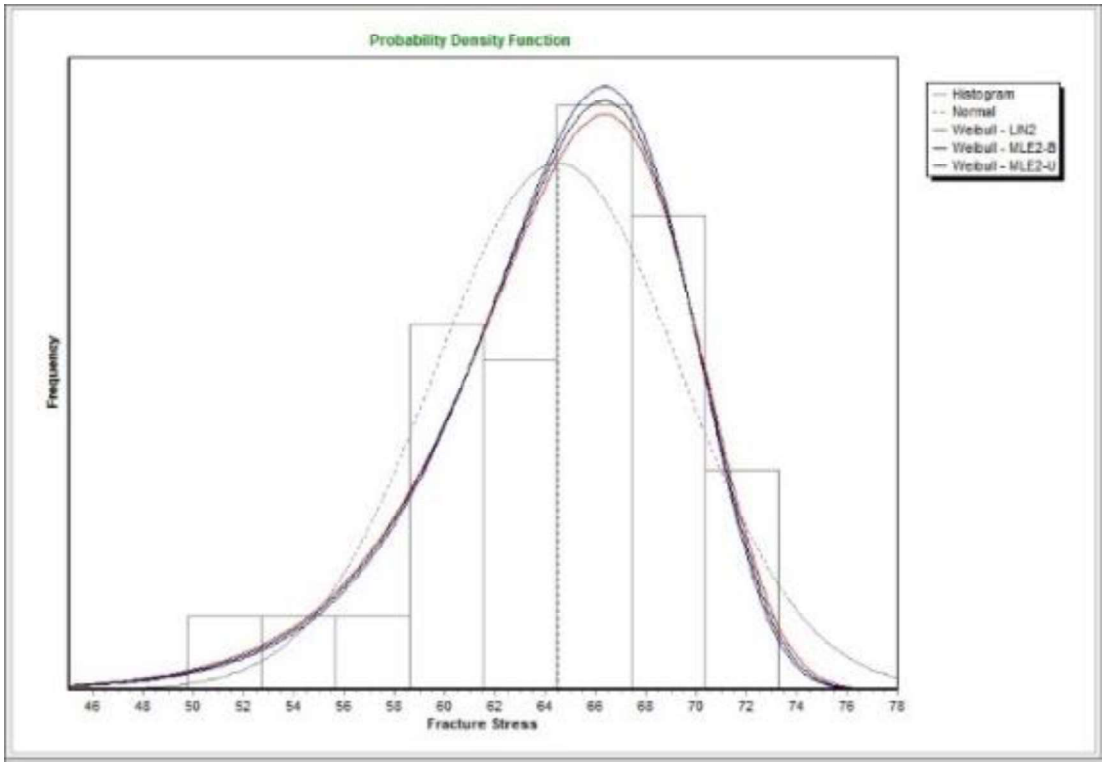

(b)

Fig. 5.22 (a) Weibull plot for large three point bend specimen best fit line for LIN2 (Linear regression with two parameter Weibull distribution), MLE2-B

(Biased maximum likelihood estimator with two parameter Weibull distribution) and MLE2-U (Unbiased maximum likelihood estimator with two parameter Weibull distribution parameter Weibull distribution) (b) Weibull PDF and Normal PDF plot and the failure strength data plot in histogram form

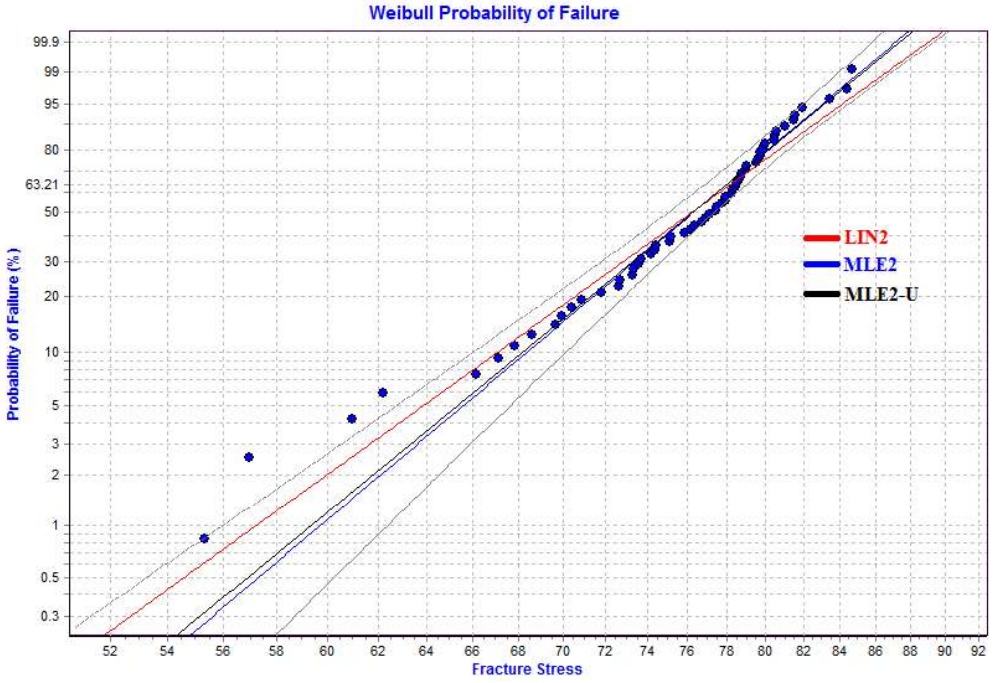

(a)

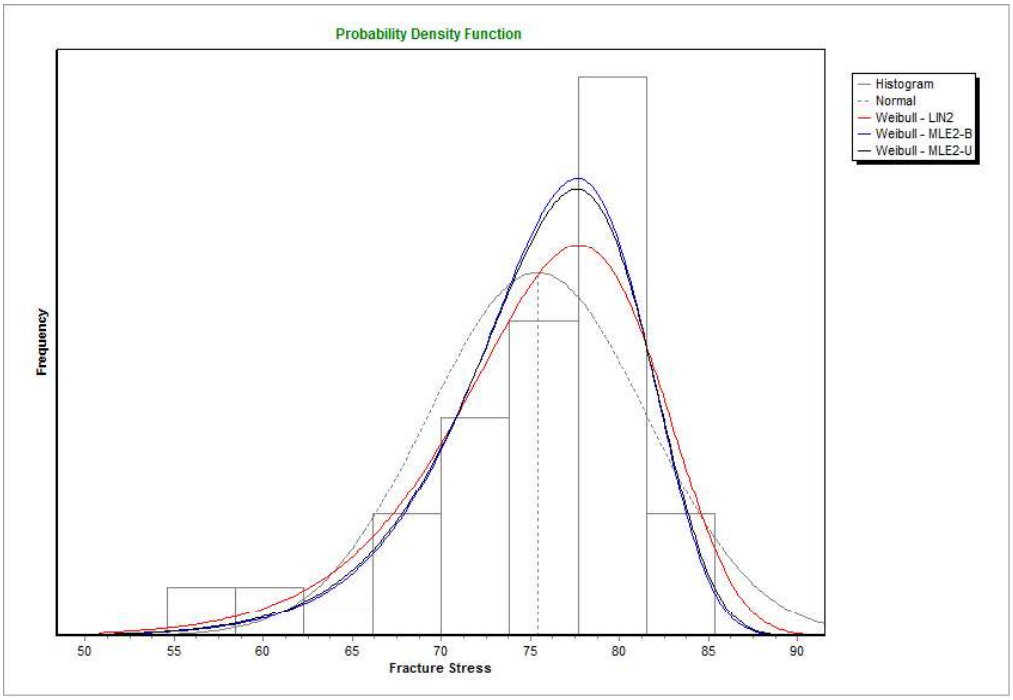

(b)

Fig. 5.23 (a) Weibull plot for small four point flexural 1/3 loading specimen best fit line for LIN2 (Linear regression with two parameter Weibull distribution), MLE2-B (Biased maximum likelihood estimator with two parameter Weibull distribution) and MLE2-U (Unbiased maximum likelihood estimator with two parameter Weibull distribution parameter Weibull distribution) (b) Weibull PDF and Normal PDF plot and the failure strength data plot in histogram form

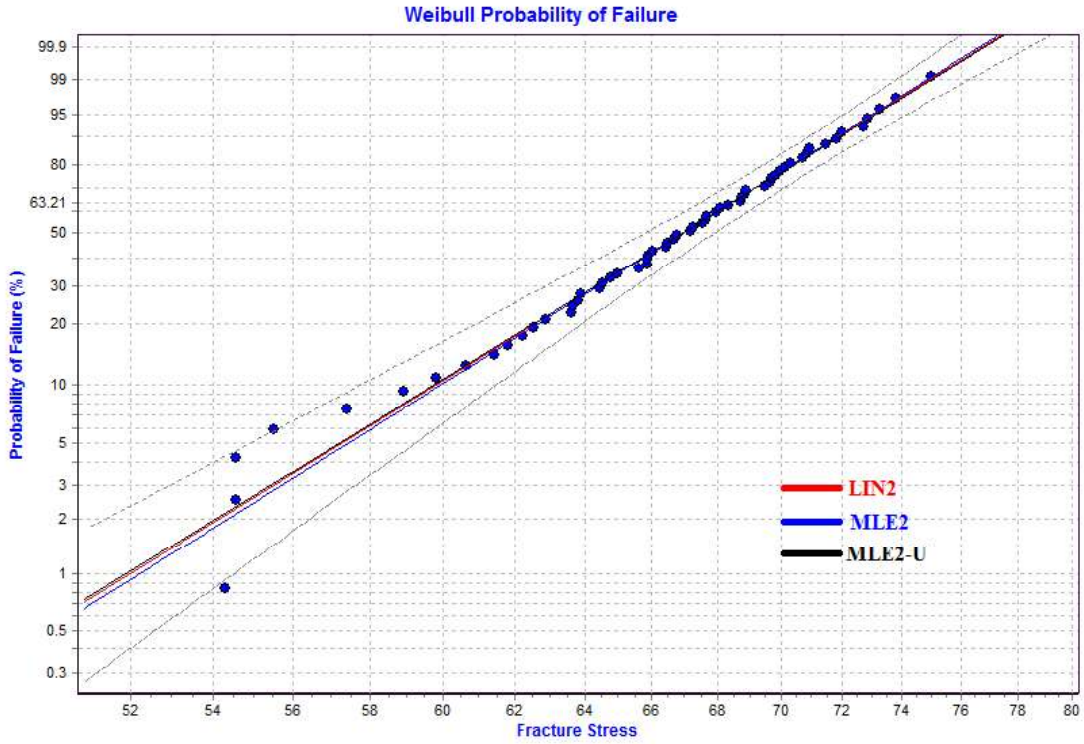

(a)

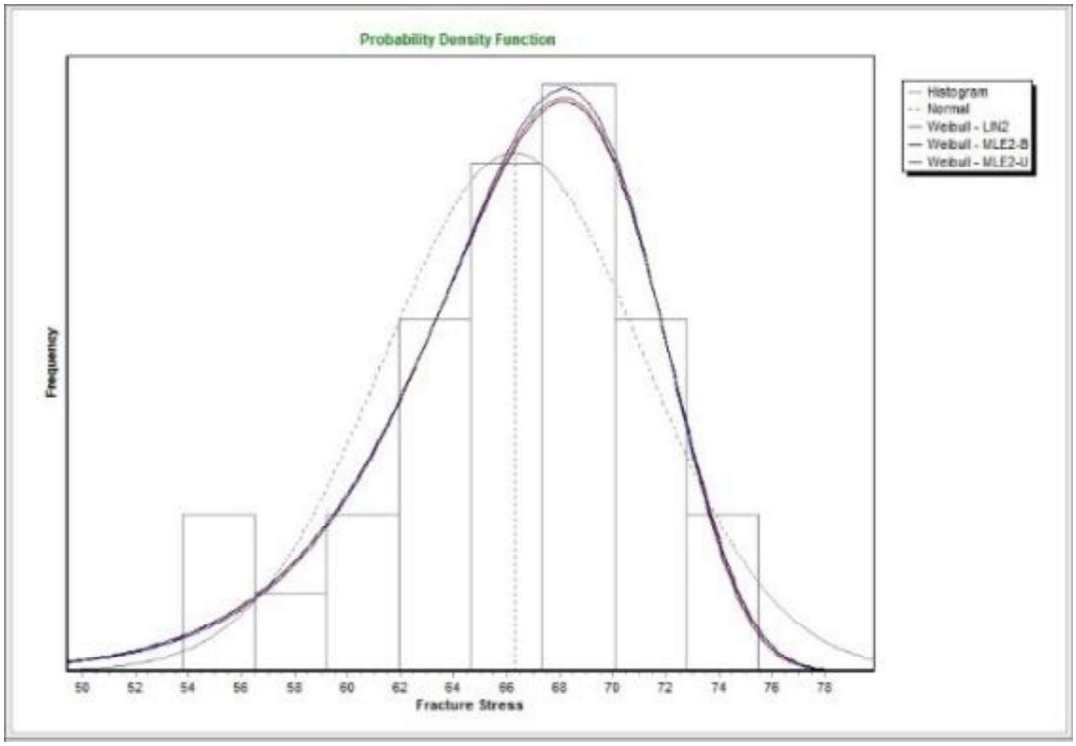

(b)

Fig. 5.24 (a) Weibull plot for large four point flexural 1/3 loading specimen best fit line for LIN2 (Linear regression with two parameter Weibull distribution), MLE2-B (Biased maximum likelihood estimator with two parameter Weibull distribution) and MLE2-U (Unbiased maximum likelihood estimator with two parameter Weibull distribution parameter Weibull distribution) (b) Weibull PDF and Normal PDF plot and the failure strength data plot in histogram form

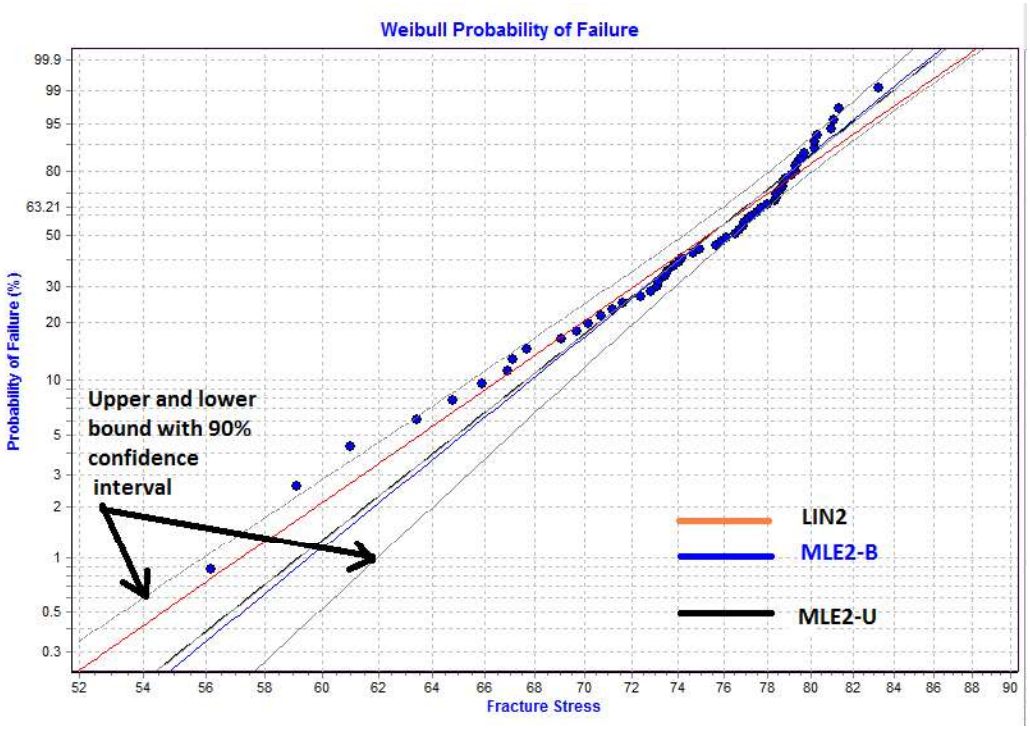

(a)

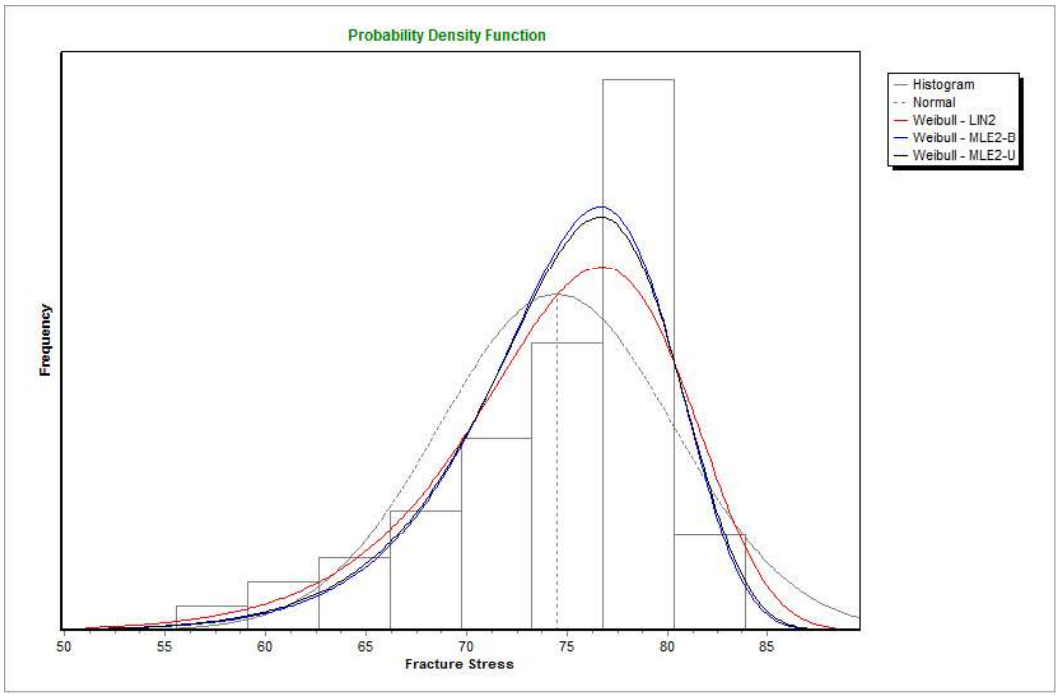

(b)

Fig. 5.25 (a) Weibull plot for small four point flexural ¼ loading specimen, best fit line for LIN2 (Linear regression with two parameter Weibull distribution), MLE2-B (Biased maximum likelihood estimator with two parameter Weibull distribution) and MLE2-U (Unbiased maximum-likelihood estimator with two

parameter Weibull distribution parameter Weibull distribution) (b) Weibull PDF and Normal PDF plot and the failure strength data plot in histogram form.

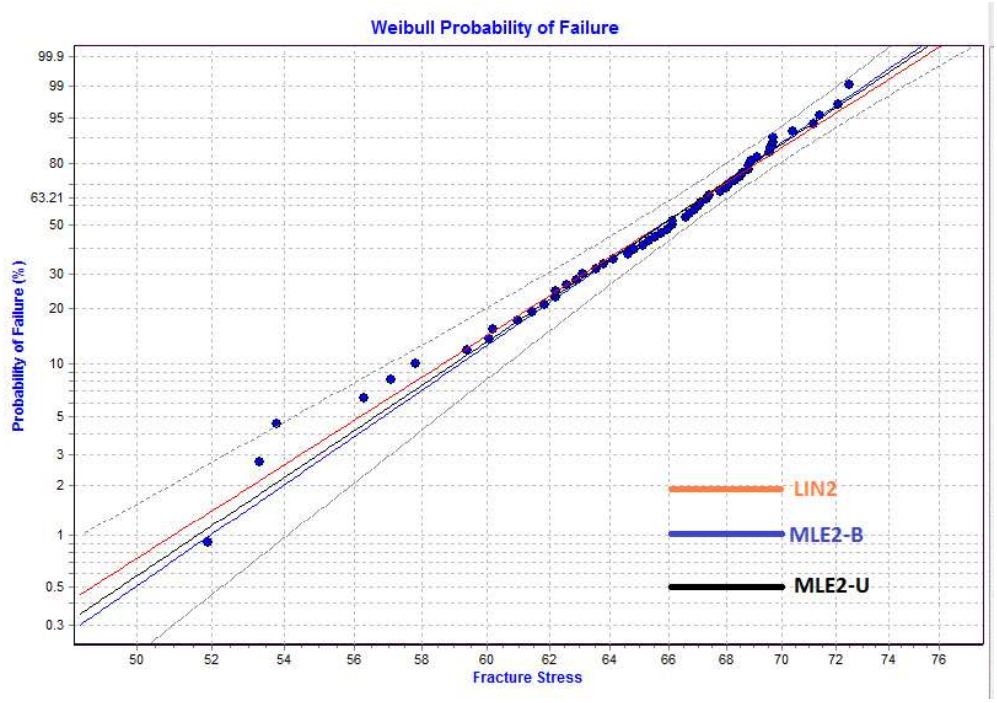

(a)

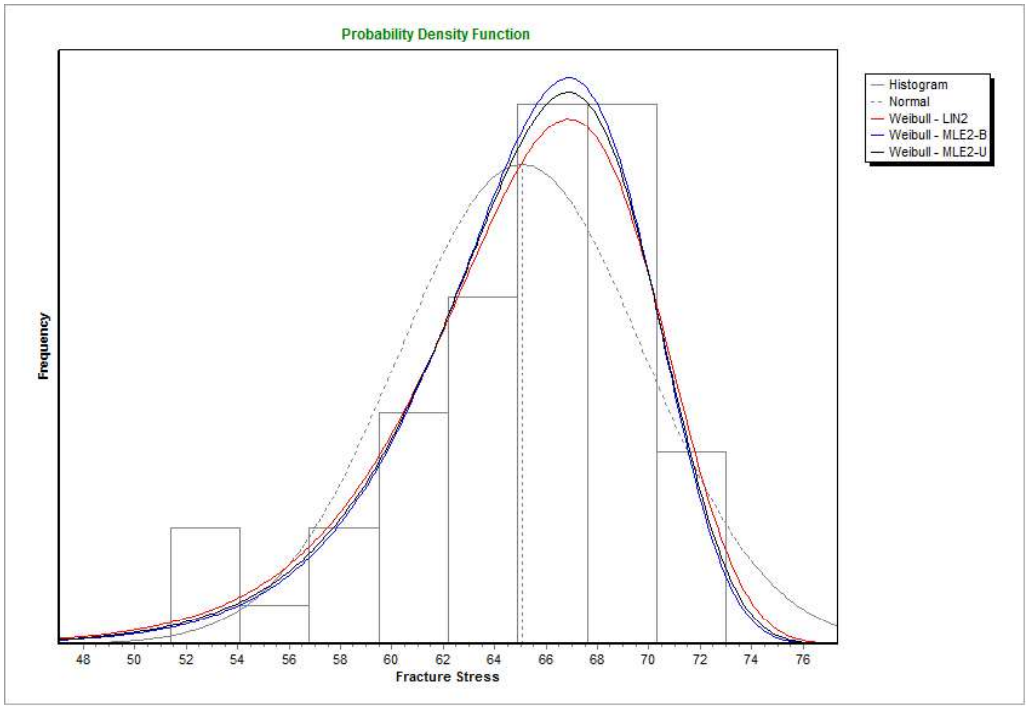

(b)

Fig. 5.26 (a) Weibull plot for large four point flexural ¼ loading specimen, best fit line for LIN2 (Linear regression with two parameter Weibull distribution), MLE2-

B (Biased maximum likelihood estimator with two parameter Weibull distribution) and MLE2-U (Unbiased maximum likelihood estimator with two parameter Weibull distribution parameter Weibull distribution) (b) Weibull PDF and Normal PDF plot and the failure strength data plot in histogram form

The two parameters Weibull distribution has been plotted with a 90% acceptable confidence level from the fracture stress data. However, a large number of test data exceeding hundred to thousand flexural experimentation might have given a better fit for the Weibull failure model. From the analysis of Weibull plot, the characteristic strength (σ_θ) and Weibull modulus (m) for the four point flexural specimen have been shown in Table 5.7.

From the Weibull plot, the goodness of fit for the failure data with their corresponding coefficient of determination (R^2 value) from Weibull parameter estimator viz: LIN2, MLE2-B, MLE2-U has been obtained and found to be more than 94% implying the sufficiency of number of test specimens for assessing the Weibull parameter. Small four point 1/4 flexural specimen test results depicted that the failure probability of the cylindrical beam with Weibull statistical distribution, two different size of flexural specimen (shown in Fig. 1) have been tested according to ASTM: D7972-14 and ASTM: C651-15. Sixty test specimen in each size has been taken for flexural testing.

Table 5.7: The characteristic strength (strength at 63.21% of probability of failure) and Weibull Modulus for large and small flexural specimen having corresponding co-efficient of determination for different loading configurations

Loading condition	Size	m			σ_θ			R^2-value		
		LIN2	MLE2-B	MLE2-U	LIN2	MLE2-B	MLE2-U	LIN2	MLE2-B	MLE2-U
3-PBT specimen	Small	16.80	17.53	17.12	75.23	75.22	75.22	.989	.987	.988
	Large	16.12	16.89	16.49	66.62	66.59	66.59	.989	.987	.989
4-PBT 1/3 loading	Small	14.77	17.25	16.84	78.09	77.89	77.90	.964	.943	.949
	Large	16.73	17.00	16.60	68.40	68.41	68.41	.979	.978	.979
4-PBT 1/4 loading	Small	15.38	17.92	17.48	77.06	76.91	76.91	0.986	0.980	0.983
	Large	16.65	17.95	17.50	67.13	67.09	67.09	0.977	0.955	0.961

The fracture test data for small and large size three point flexural specimens sets, four point 1/3 flexural specimens and four point 1/3 flexural specimens are used in developing Weibull plots. The Weibull plot for the respective flexure specimen is delineated in Fig. 5.21 to 5.26 for small and large bend specimen and best possible fit line using Linear regression, biased maximum likelihood estimator and unbiased maximum likelihood estimator with two parameter Weibull distribution have been presented. The blue dots are the actual data sets and red line represents the linear regression whereas the blue and black line shows the best fit line by maximum likelihood biased and unbiased estimator.

The characteristic strength (σ_θ) and Weibull modulus (m) for large and small tensile specimen have been collected in Table 5.7 after analysis of plots in Fig. 5.21(a) to 5.26(a). It is noticed that the behaviour of three point specimens have slightly lower strength than the four point flexural specimens. Also Weibull modulus variation between small and large specimen is very less signifying its

material constant value for the tested specimens. The Figure 5.21(b) to 5.26 (b) illustrates the failure data in the form of histogram and probability distribution function plot based on Normal and Weibull distribution with three estimators as LIN2, MLE2-B and MLE2-U in the form of dotted and full bell shaped lines. It has been seen clearly that Weibull distribution fits better than the normal distribution for the experimental data. CARES and WeibPar software code is used to compare and validate semi analytical results for effective volume and effective surface from the experimental fracture data. Some post processing code has been developed which takes the input results from finite element bimodular model simulation using general purpose COMSOL FE software for the validation of bimodular graphite fracture data with the Newton-Raphson solution of analytical integral formulation developed earlier in Table 5.2 and 5.3.

The stress, strain, deformation and geometry data of bimodular finite element model results file of COMSOL finite element program is imported to Fortran programming for evaluating Weibull effective surface and effective volume based on the Principle of Independent Action. The principal of independent action (PIA) is taken as fracture criteria for the analysis. The same has been carried out for all category of flexural specimen considering both unimodular and bimodular elastic characteristics. Also, the effective volume of the cylindrical specimen is evaluated by CARES and WeibPar software considering the material as unimodular and compared with the unimodular effective volume calculated from Quinn's derived formula (Quinn 2003a) and the mode difference is found to be 9.57% and 8.92 % for small and large flexural specimen with Four Point Bend 1/4 loading. Similar error percentage for each category has been noted for both the Weibull effective

surface and volume. Typically for effective surface area the error percentage with bimodular model is much less than that of unimodular assumption.

Table 5.8 Effective volume tabulation for analytical and experimental analysis

Flexural Loading condition	Size	Calculated from integral in the present work (mm^3)	Developed FE Model and post processing code (mm^3) using bimodular Experimental Flexure Test data	Mode Error (%)	Calculated from CARES and Weibpar (mm^3) from unimodular FE model unimodular Experimental Flexure Test data	Calculated from above integral for unimodular assumption (mm^3) Quinn's paper Formula (Quinn 2003a)	Mode Error (%)
3-PBT specimen	Small	1.88	1.96	4.25	2.01	2.15	6.51
	Large	16.47	16.86	2.31	17.32	18.80	7.87
4-PBT 1/3 loading	Small	13.19	13.46	2.04	14.01	15.09	7.15
	Large	107.84	109.72	1.74	115.26	123.37	6.57
4-PBT 1/4 loading	Small	17.51	17.21	1.71	18.03	19.9889	9.57
	Large	139.99	138.01	1.14	145.31	159.65	8.92

Table 5.9 Tabulation of Effective volume for analytical and experimental analysis

Flexural Loading condition	Size	Calculated from integral in the present work (mm^2)	Calculated from FE Model and post processing code (mm^2)	Mode Error (%)	Calculated from Cares and WeibPar (mm^3) Using Unimodular assumption (mm^2)	Calculated from above integral for unimodular assumption (mm^2) Quinn's paper Formula (Quinn 2003a)	Mode Error (%)
Three point bend specimen	Small	7.82	7.95	1.66	8.05	8.32	3.2
	Large	33.02	33.56	1.63	33.96	34.76	2.44
Four Point Bend 1/3 loading	Small	54.05	53.56	0.90	55.01	56.89	3.30
	Large	218.01	219.74	0.79	237.46	229.46	3.48
Four Point Bend 1/4 loading	Small	74.48	74.98	0.67	76.12	77.87	2.23
	Large	298.75	300.02	0.42	304.57	311.31	2.29

A detailed comparison of Weibull effective volume and Weibull effective surface area with and without bimodular material consideration for small and large flexural specimens is provided in Table 5.8 and 5.9. Comparing all columns in these table, it is seen that column 4 demonstrating the use of bimodular test data in

Weibull effective volume and surface evaluation is more close to the predicted analytical integral data (Column 3 of Table 5.8 and 5.9) derived in this work in comparison to column 6 (CARES unimodular model) and Column 7 (Quinn's unimodular model). Therefore appropriate design corrections are necessary for assessing the structural integrity of bimodular material made structures.

5.6 Conclusions

In the present work, the semi analytical expressions for Weibull effective volume and surface area for beam of circular cross section possessing bimodularity and loaded in different flexural configuration have been derived. In a bimodular beam, neutral axis is shifted from centroidal axis and thereby volume in tension and maximum tensile stress in the specimen are different as compared to the unimodular case and hence cause changes in the Weibull effective volume and effective surface area. This has been reflected in the Weibull effective volume and effective surface plots. Characteristic bimodular parameter α (E_T/E_C) has a significant effect on the asymtotatic variation of Weibull volume/surface vs Weibull modulus variation. This suggests the importance of bimodularity for high risk bimodular material structures. Additionally, it has been shown that strength scaling ratios are independent of whether the flaws are volume or surface distributed for the beams having same cross-sectional shape and size. Conversion factors have been tabulated for different flexural configurations. Weibull model has been developed using concept of weakest link for experimental validation of proposed integrals for effective volume/ surface area. Experimentations have been conducted to assess the Weibull characteristic strength and Weibull modulus for bimodular high purity graphite specimens with a 90% confidence bound level

with the help of Weibpar and CARES software using appropriate finite element model. A post processing code has been written in FORTRAN language to quantify the effect of bimodularity. It is perceived from Weibull models developed for experimental data sets that it is difficult to prove experimentally the effect of bimodularity on three point bend specimens because of comparatively low value of effective volume and surface area, whereas for the four point bend specimen, proposed integral matched more convincingly with the bimodular Weibull model value. Some small errors (between Column 3 and Column 4, Table 5.8 and 5.9) have been reported between analytical and experimental effective volume/surface comparison which might be attributed to the lower sample size of fracture test data undertaken in the analysis. Nevertheless, consideration of the influence of bimodularity has minimized the error percentage between predicted analytical integral formulation and experimental evaluation.